INSTIITUTE OF ACCELERATING SYSTEMS AND APPLICATIONS, ATHENS, GREECE
WP10 Coordinator

MEDITERRANEAN OCEAN FORECASTING SYSTEM: TOWARD ENVIRONMENTAL PREDICTION

MFSTEP

Project Deliverable Report
D16

WP10: Atmospheric Forcing and Air-Sea Interaction Studies

Project title	**MEDITERRANEAN OCEAN FORECASTING SYSTEM: TOWARD ENVIRONMENTAL PREDICTION**
Project acronym	**MFSTEP**
Contract number	**EVK3-CT-2002-00075**
Deliverable number	**D16**
Deliverable title	**Skill scores for the various models and their configuration**
Work package	**WP10 Atmospheric Forcing and Air-Sea Interaction Studies**
Name of WP10 Coordinator	**Prof. George Kallos Institute of Accelerating Systems and Applications, Athens, Greece**
Date of delivery	**May 2006**
Report status	**Version 1.0 Draft Final X**
Project home page	**http://www.bo.ingv.it/mfstep/**

1 Introduction

This report describes the work performed by IASA and ICoD under the scopes of deliverable 16 (subtask 10510) of WP10. This WP contained the necessary activities to create and deliver the atmospheric surface fields to the WP8 and WP9 ocean modeling community, to examine the sensitivity of atmospheric response to sea surface temperatures, to study the air-sea interactions and to implement higher resolution limited area models in Mediterranean sub-regions. Moreover, one of its more important aims was to define and perform the Scientific Validation Period (SVP) intercomparison of atmospheric models. This deliverable presents the configuration of the limited area atmospheric models utilized in the intercomparison, the employed statistical methods and the skill scores of the various models.

2 Model Configuration

The three numerical models that were used in the validation studies of subtask 10510 were SKIRON/Eta, Aladin/MFSTEP and NMM models, and they are described here. The SVP hindcasts of SKIRON/Eta and Aladin/MFSTEP were provided to the MFSTEP partners for the experiments of the wave and ocean models. These two models also provided operational forecasts during MFSTEP.

On the other hand, the SVP hindcasts of NMM were not disseminated to the MFSTEP partners. According to the DoW, only the SKIRON/Eta and Aladin models were planned to provide their SVP output to the ocean modelers. However, the validation of NMM was necessary (in subtask 10510) since this model was utilized in a number of subtasks (e.g. 10310, 10420).

2.1 SKIRON/Eta

The SKIRON/Eta modeling system was developed for operational use at the AM&WFG/IASA. The implementation of the system requires Unix computational environment and corresponding meteorological data input. The current version of the Eta model is appropriately coded in order to run on any parallel computer platform utilizing any number of processors (Kallos et al. 1997b). The system was developed in order to operate as fully automatic.

The SKIRON/Eta system is based on the Eta/NCEP model. A detailed description of its characteristics and configurations is to be found in Kallos (1997), Nickovic et al. (1998), Papadopoulos et al. (2002) and others.

The model has several unique capabilities making it appropriate for regional/mesoscale simulations in regions with varying physiographic characteristics. It has the unique capability to use either a "step-mountain" vertical coordinate (Mesinger 1984) or the customary pressure or sigma (or hybrid) coordinate. The SKIRON/Eta modeling system is also including dust cycle capabilities. The hydrostatic version of the system is successfully used operationally in the University of Athens since 1997, as well as in applications of simulations of historical dust-storm events (Nickovic et al. 2001). During the last years, mercury cycle modules have also been incorporated to the SKIRON/Eta system providing forecasts of the concentration and deposition of mercury in Europe and USA (Kallos et al. 2001; Voudouri et al. 2005).

The main features of the system that was implemented in the Mediterranean region in the framework of MFSTEP project are briefly described in the following sections.

2.1.1 Model geometry and dynamics

- The model variables are represented on the staggered Arakawa E-grid. It has been shown by Winninghoff (1968) and Arakawa and Lamb (1977) that various horizontal grids simulate differently large and synoptic scale atmospheric processes. It was demonstrated that the grids E and C (and also the B grid which is equivalent to E) have advantages relative to the A and D grids. The grid separation related to the E grid is avoided by the use of a special technique (Mesinger 1973; Janjic 1974, 1979).
- For horizontal advection the cascade process of non-linear energy toward smaller scales is under control.

- The "step-mountain" Eta coordinate is used in the vertical. The eta coordinate system is proposed as a response to a problem related to the sigma terrain-following coordinate when applied to steep mountain areas. This problem appears as a result of the errors associated with the implied vertical interpolation of geopotential from sigma to pressure surfaces and can generate significant errors in the vicinity of the steep model mountains. In contrast to the sigma surfaces, the constant eta coordinate surfaces are quasi-horizontal in both mountainous and non-mountainous areas. Thus, it may be considered that the eta coordinate represents a more natural alternative to the widely used sigma system for ever-increasing horizontal and vertical model resolution, accompanied by a need to have more realistic model mountains.
- The arithmetic solution of the set of equations is performed in a grid point model using a finite difference scheme.
- A split-explicit scheme is used for time differencing. More specifically, a “forward-then-centered time” time differencing scheme is used for the horizontal advection. For the vertical advection of temperature, specific humidity, turbulent kinetic energy and horizontal momentum, the Euler-backward (Matsuno) scheme is used.
- The model includes the option to use either the hydrostatic assumption or nonhydrostatic dynamics. In the framework of the MFSTEP project the model physics included nonhydrostatic dynamics (Janjic et al. 2001). The nonhydrostatic model appears to be computationally robust at all resolutions and efficient in NWP applications. The use of nonhydrostatic dynamics is an important improvement for very high-resolution simulations in which the non-hydrostatic processes may exert a significant influence on the meteorological fields. In high-resolution simulations the nonhydrostatic model is generally more robust than the hydrostatic one and produces smoother solutions.

2.1.2 Physical parameterizations

There is a large number of physical processes that cannot be explicitly modeled despite the high horizontal resolution that was used in the MFSTEP forecasts. These processes are included in the model through parameterization schemes. In the SKIRON/Eta model there is a large number of such schemes:

- The boundary layer is parameterized using a 2.5 order closure scheme proposed by Mellor and Yamada (1982).
- A 2nd order closure scheme proposed by Mellor and Yamada is used to parameterize the surface layer.
- A viscous sublayer scheme is used over ground and water surfaces in order to improve the calculation of the surface fluxes. The method proposed by Zilitinkevich (1995) is used over ground points, specifying an effective roughness length as a function of the flow regime and of the grid-box orography variation. The viscous sublayer over water surfaces in the Skiron/Eta model is designed by matching the log profile of the considered variables with a separate viscous sublayer profile (Janjic 1994).
- The surface and soil processes are parameterized using the OSU scheme. The soil temperature and moisture are calculated at six layers extending from the surface down to 255cm. A data assimilation scheme for soil temperature and soil wetness was recently developed.
- The parameterisation of the subgrid scale convective processes is allowed to use either the modified Betts-Miller-Janjic or the Kain-Fritsch approach. Both schemes take into account deep and shallow convection. In the framework of MFSTEP project, the model was integrated using the Betts-Miller-Janjic convective parameterization.
- The large-scale cloud and precipitation parameterization is based on the scheme of Zhao and Carr (1997). In this scheme cloud water and ice are prognostically calculated in the stratiform clouds. Precipitation is diagnosed directly from the cloud water/ice content. Two types of precipitation, rain and snow, are calculated in the scheme. Evaporation of clouds and precipitation and snow melting below the freezing level are allowed by the model.
- The radiative fluxes are calculated using the GFDL radiation scheme (e.g. Schwarzkopf and Fells 1991). Three radiatively active gases of the atmosphere (water vapour, carbon dioxide and ozone) are considered. The GFDL scheme takes into account the cloud information supplied by the parameterization of moist processes allowing random overlapping of clouds at various levels.

2.1.3 Surface characteristics

High resolution topography, vegetation and soil data are used. The topography and vegetation data are available from USGS with a resolution of 30x30 arc sec, with the later following the SiB classification (Dorman and Sellers 1989). For soil textural class the UNEP/FAO dataset (2x2 arc min) is used after its conversion from soil type to soil textural ZOBLER classes (Zobler 1986).

The model also allows the use of high resolution NCEP SST data of 0.5 degrees, or SST data from other sources, high-resolution NESDIS snow and ice cover data and US Air Force snow depth analysis data. These products are available daily in standard WMO grib format.

The NCEP SST dataset is produced on a 0.5° (latitude-longitude) grid by an optimum interpolation analysis of the most recent 24-hours receipts of buoy and ship data, satellite-retrieved SST data and SSTs derived from satellite-observed sea ice coverage. The SKIRON/Eta modeling system was been prepared to use alternatively the lower resolution (1°) NCEP SST dataset and the 0.5° ECMWF SSTs. It has been shown that the use of the high resolution SSTs by ETA model resulted to improved forecasts of storm track and precipitation over Eastern US (Thiebaux et al. 2003). Sensitivity tests performed by the SKIRON/Eta model during the pseudo-operational mode runs indicated the superiority of the 0.5° SSTs. The importance of high resolution SST data in high resolution modeling in the Mediterranean region was investigated extensively in MFSTEP project.

2.1.4 Model domain

The computational model domain covered the whole Mediterranean Region and part of Central Europe (Figure 1). In the horizontal, a grid increment of 0.1 degrees was applied. Because of the high horizontal resolution a timestep of 30 sec was used. In the vertical, 38 levels were used stretching from the ground to the model top at 25 mb (corresponding approximately to 25 km).

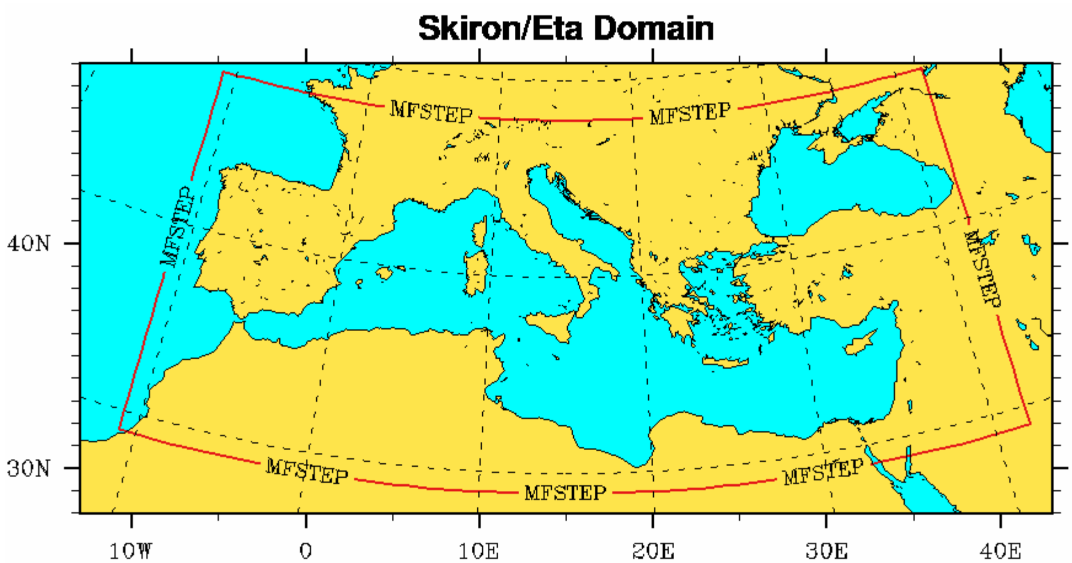

Figure 1. *The computational and dissemination (framed) model domain of Skiron/Eta modelling system.*

2.1.5 Initial and Boundary conditions

During the TOP SKIRON/Eta and Aladin models produced 120-hour forecasts initialized every Wednesday from the 0000 UTC ARPEGE analyses. In the SVP hindcasts the forecast horizon was 72 hours. In SKIRON/Eta the initialization of the soil moisture content and the soil temperature was performed using the 24-hour forecast of the run of the previous day. The sea-surface temperature field was forced by the daily 0.5° latitude x 0.5° longitude NCEP SSTs and it remained fixed to its initial value throughout each simulation. The lateral boundary conditions were based on the ARPEGE forecasts and were updated every 3 hours. The ARPEGE analyses and forecasts used for initial and lateral boundary conditions were provided by Meteo-France at a horizontal resolution of 0.25x0.25 degrees.

2.1.6 Computer resources

The high-resolution SKIRON/Eta modelling system run at the computer facilities of IASA. Specifically, a cluster of ten (10) dual-CPU nodes based on ATHLON-1900 processors was used and was configured in order to handle large data storage, namely a RAID 4:1 system handling approximately 350 GBYTE of data on line. The system was exclusively available for the scope of the project. The system is connected to a high-speed network (1 Gbit/sec the slowest network section). The SKIRON/Eta modeling system run parallel in order to achieve the highest performance.

2.2 Aladin/MFSTEP

2.2.1 Introduction

For the purpose of fulfilling the objectives of Work Package 10 of MFSTEP, a special configuration of the ALADIN NWP system run in dedicated mode on the SX6 computer of CHMI-Prague. The basic constraints of the TOP final set-up were the following: (i) running a permanent ALADIN pseudo data assimilation cycle in full coupling with the 4D-Var long-cut-off cycle of the ARPEGE global NWP system of Météo-France in Toulouse (6 hour updating frequency in both cases, coupling every three hours, hourly output frequency for the atmosphere-ocean coupling data); (ii) once a week on Wednesday 00 UTC, launch of a 5 day ALADIN adaptation forecast coupled with a special run of ARPEGE based on the above-mentioned assimilation cycle (same conditions of coupling and production as above); (iii) an option was considered in which SST results from the OGCM could enter the step ‘i’.

The system run on a 589 x 309 domain with a mesh size of 9.508 km (5591 x 2928 km2 hence; Figure 2). The projection was a Lambert tangential one (reference point 46.47N-2.58E) and the centre of the domain was at 41.95N-9.81E. There were 37 vertical levels irregularly spaced in the so-called ‘hybrid-eta’ coordinate of Simmons and Burridge (1981), the top one being at 5hPa and the bottom one at about 17 meters above the surface. The elliptic spectral truncations were E299/159 (linear-grid) for the forecasting model and E83/44 for the filtering part of the so-called blending procedure. The time-step was 400 seconds.

The post processing was done on a lat/lon grid of 0.1 degree in each direction with limits at 19W, 37E, 30N and 48N (Figure 2).

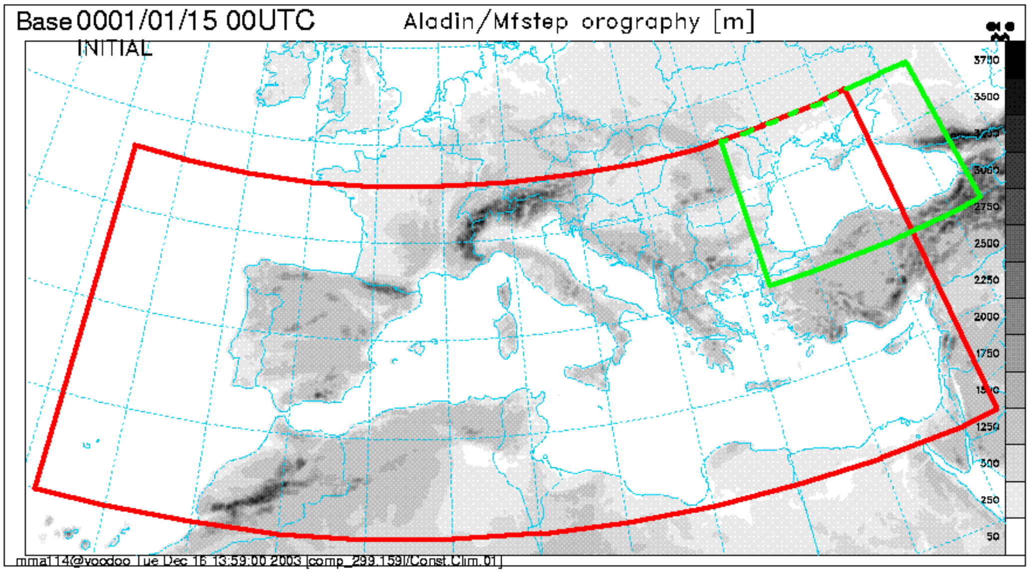

Figure 2. *The computational domain of Aladin model and the associated orography. The two color frames encompass the dissemination domains of Meteo-France and CHMI for the Mediterranean and the Black sea.*

2.2.2 Dynamical part

The ALADIN Hydrostatic Primitive Equations (HPE) dynamics is the transcription to the Limited Area Modelling (LAM) world of the IFS/ARPEGE global one, jointly developed by ECMWF and Météo-France. The jump from the spherical geometry to the tangential plane one is accomplished following the idea of Machenhauer and Haugen (1987) which allows to keep all the advantages of the spectral approach at minimum overhead costs (see Geleyn, 1998). The vertical discretisation is the one advocated by Simmons and Burridge (1981). The semi-implicit, semi-Lagrangian two-time-level time-marching scheme is quite close to the one described in Ritchie et al. (1995), Simmons and Temperton (1997), Ritchie and Tanguay (1996) and Hortal (2000), with two ARPEGE/ALADIN enhancements: the implicit treatment of the Coriolis term as proposed by Rochas (see Temperton, 1997) and an analytical (rather than interpolated) computation of the coordinates of the origin point of the trajectories. This scheme allows the use of the so-called ‘linear grid’ (see Côté and Staniforth, 1988), i.e. a reduction to its minimum of the spectral aliasing problem, as well as very efficient time steps (Courant numbers down to 23 m/s).

For the reasons explained in McDonald (1998), the orography (still of 'envelope' type for the time being, see below) is fitted like for a classical quadratic grid, but applying the method of Bouteloup (1995) spectacularly reduces the Gibbs effects over sea.

The horizontal diffusion is implicit linear and fourth-order with a divergence damping factor of five. The e-folding time of the smallest wave for vorticity, vertically scaled temperature and moisture is set proportional to the model mesh-size with a ratio of 12.3 m/s in the linear-grid case. This value is the one for the surface and the effect increases with height in inverse proportion to pressure.

The lateral coupling of the LAM is of the Davies (1976) type and its interaction with the semi-implicit procedure is performed at no additional cost thanks to the suggestion of Radnoti (1995).

Beside the HPE version, there exists a non-hydrostatic fully compressible version of ALADIN (Bubnova et al., 1995) following the suggestion of Laprise (1992) to keep the HPE continuity equation unchanged through the use of a hydrostatic-pressure-based vertical coordinate. However, this was not used in the basic MFSTEP set-up, owing to its very small impact at 10 km of mesh-size.

2.2.3 Physical Parameterizations

Radiation computations

The basic scheme is adapted from Geleyn and Hollingsworth (1979) and Ritter and Geleyn (1992) and simplified enough for being able to describe the interactions soil-radiation and clouds-radiation at each time step. The three main 'compromise' hypotheses for speeding-up the calculations are the following:

- only one spectral interval in the solar as well as in the thermal range, but consideration of all active gases as well as of the separation between liquid- and ice-cloud components;
- grey body assumption (i.e. linear monochromatic behaviour) for all effects except gaseous absorption (but multiple scattering is treated without approximation, even in the thermal domain, thanks to a delta-two-stream computation with a choice between random and maximum-random (unused) overlap hypothesis for cloud geometry);
- the interaction between line absorption of gases and two-stream 'adding' method as well as the saturation effects of the former are treated via the diagnostic estimation of a 'minimum' gaseous optical depth for all remaining effects, once (i) absorption of parallel solar radiation in the solar domain and (ii) so-called 'cooling to space' and 'exchange with surface' terms in the thermal domain have been treated exactly.

The diagnostic schemes for the 'radiative' clouds link the cloudiness to the production of stratiform and convective precipitations, and to the existence of inversions. The scheme is based on the following principles:

- cloudiness functionally depends (with different parameters for the stratiform and convective contributions to a single amount) on the diagnosed liquid- ore ice-water-content; the functional dependency is one of those proposed by Xu and Randall;
- the contribution is obtained from the rate of generation of convective precipitation at the previous time step in one case;
- in the other case, one estimates the instantaneous super-saturation of the air properties averaged along a certain delta-theta thickness below, with respect to the local saturation state multiplied by a 'critical relative humidity' vertical profile (tuned with two parameters only);

the partition between ice and liquid state depends only on temperature with a progressive transition below 0°C.

One is currently considering a new structure for the radiative computations in which the clear sky gaseous computations, the cloud/aerosol sub-model and the delta-two-stream solver would be considered as three independent parts, this allowing more flexibility and a different view of the 'radiative time stepping problem'.

Turbulent vertical diffusion and PBL

The common scheme for the surface and upper-air exchanges is designed according to Louis (1979) and Louis et al. (1981), with the shallow convection incorporated according to Geleyn (1987) and recently modified to cure a tendency to an on/off behaviour in time and along the vertical. For the past four years a big effort (still on-going) has been made to improve the coefficients' dependency on the Richardson number in case of stable situations. Two (positive) critical Richardson numbers (each with a potentially modulated vertical profile) have been introduced. The first one deals with the enhancing effect on fluxes of sub-grid inhomogeneities and the second one with the difference in the effect of such inhomogeneities between the thermal and momentum parts of the calculation.

A retuning of the 'mixing length' vertical profile was applied during this work and it is intended to make it dependent at some stage on the time- and space-dependent height of tropopause and PBL depth, the latter computed according to Ayotte.

The residual gusts when the wind is weak near the sea surface and the situation is unstable are treated via a stability-dependent enhancement of the result of the basic Charnock formula, in the spirit of the work of Miller. An enhancement to the moist convective case, inspired by the ideas of Redelsperger is currently considered as well as the possibility to distinguish between roughness lengths for momentum and for heat over sea (as it is already the case over land).

The 'anti-fibrillation' scheme of Bénard et al. (2000) is activated. Extending the idea of Girard and Delage, it introduces an over-implicit treatment only when and where the linear local full stability analysis estimates it necessary in order to get a pre-chosen degree of 'smoothness' of the solution. In order to avoid getting 'space-sliced' patterns in place of time oscillations, a constraint of vertical monotonicity was recently imposed on the resulting over-implicit factor. Since this scheme, by construction, cannot handle the type of shallow convection parameterisation via turbulent exchange coefficients' enhancement used in the package, the above-mentioned modification of the shallow convection scheme had to be introduced to harmonise the whole treatment.

Specific diagnostics for the boundary layer are (in a broad sense and were adapted to MFSTEP specificities during the SVP):

- interpolated values in the SBL (generally towards the measurement heights);
- PBL height (up to now computed with a Richardson number offset, soon to be replaced by the above-mentioned adaptation of Ayotte's method);
- maximum gust wind speed, either through a link with the dynamical roughness and the surface friction velocity or as the wind at the top of the PBL;
- CAPE and moisture convergence (several algorithmic options for each of them) computations for the instantaneous diagnostic of convective risk, especially in diagnostic mode with a frequent near-surface-analysis update.

Mountain drag scheme

It describes in a broad sense the influence of unresolved orography on the higher levels of the atmosphere in a way adapted from Boer et al. (1984) for the linear 'gravity wave drag' part (with full use of the Lindzen (1981) saturation criterion for applying the Eliassen-Palm theorem) and from Lott and Miller (1997) for the 'form drag' low level part. An optional (yet unused) parameterisation of the sub-grid scale so-called 'lift' effect exists, following Lott (1999). Some additional effects are taken into account for the following aspects:

- influence of the anisotropy of the sub-grid orography on the direction and intensity of the stress, according to Phillips;
- use of averaged wind and stability low level conditions (and smooth return to the true profiles above the averaging depth) in order to get a surface stress as independent as possible of the model's vertical discretisation;
- amplifying or destructive resonance effects parameterised according to the work of Peltier and Clark, as well as dispersion effects in case of upper-air neutrality;
- the linear and non-linear potential instabilities of this complex scheme are preventively eliminated at the time of computation of the integrated effects (except for the 'lift' case that is currently an independent piece of parameterisation put in the scheme's code only for convenience).

Deep convection

This parameterisation is surely the one that has received most attention in the evolution of the considered physics package. Contrary to the general tendency in other NWP groups, most of the attention has been paid to the formulation of the entrainment and to its consequences and not to the closure assumption, still of the Kuo-type, even if its practical implementation has also gone more complex than in the 80's.

The original scheme is the mass-flux-type one from Bougeault (1985), modified for the numerical stability according to the Appendix of Geleyn et al. (1982). In its current version it encompasses the following refinements:

- the Kuo-type closure has been made dependent on the horizontal resolution according to the ideas of Bougeault and Geleyn since the dynamical part of the moisture convergence is here modulated by a factor depending on the mesh size and that goes to zero for a vanishing one;
- a very simple microphysics to avoid 'deep convection' from too shallow clouds; this follows the proposal formulated in the Appendix of Arakawa and Schubert;
- it is forbidden to have deep convection when absolute dry convection is active;
- a comprehensive treatment of the vertical transport of horizontal momentum that includes the recirculation by the mass-flux in the Schneider and Lindzen sense, the effect of lateral entrainment and the effects of pressure difference between the cloud and its environment following the proposal of Gregory; the 'non-hydrostatic' part of the moist adiabat ascent/descent computations are treated in conformity with Gregory's underlying hypotheses;
- a provision for cancelling the computations when the potential for convective rain at the surface makes it unlikely for the ascent to reach the lifting condensation level;
- a vertically varying detrainment rate with a constant component plus a dependency on the buoyancy decrease in the upper part of the cloud;
- an entrainment rate that (i) varies from higher values at the bottom to lower ones at the top alike the proposal of Gregory and Rowntree, (ii) is dependent on a first estimate of the integrated buoyancy and (iii) encompasses the 'ensembling entrainment' concept (i.e. the clouds inside a grid-box that survive at a given height have a higher buoyancy than

the averaged one below, because they entrained less in their lower part) in its consequences on the profiles;

- parameterisation of downdrafts via quasi-symmetric computations for the ascending and descending motions following Ducrocq and Bougeault; the additional differences are a geometric modulation of the mass flux to avoid its convergence in the sole lowest model level and constant entrainment/detrainment rates along the vertical, contrary to the description in the last two bullets, valid only for updrafts;
- in the closure assumption for the downdraft part, precipitation fluxes' creation replaces moisture convergence but Bougeault's main closure coefficient (ratio of mass flux to buoyancy) has been constrained to remain smaller for downdrafts than for updrafts in order to avoid a runaway feedback when a shallow moist unstable layer caps a deep dry and well-mixed PBL; to alleviate the consequences of this 'security' in terms of surface fluxes a compensating 'unorganised' sub-cloud evaporation term is incorporated following a relaxation method.

Stratiform precipitation scheme

There is neither storage of the liquid and solid phases in the clouds, nor consideration of partial cloudiness, but a revised Kessler (1969) method is used for computing precipitation evaporation, melting and freezing. A ratio of the falling speed for the two types of precipitation allows distinguishing two aspects in the liquid/ice partition:

- formation that follows the same partition as the one used in the radiative diagnostic cloud scheme;
- evolution for the falling parts that takes into account the past 'history' of the falling fluxes, even if those are diagnosed under a (time-step by time-step updated) stationarity assumption.

Parameterisations of the soil processes

This is based on the ISBA scheme described by Noilhan and Planton (1989) and by Giard and Bazile (2000). Some modifications have been added to the scheme for taking into account the freezing-melting effects of the soil water at different levels. The research version of the same scheme is well known through the participation to the various international inter-comparisons (PILPS, SNOWMIP, …).

2.2.4 'Pseudo-data assimilation' part

Upper air blending

The initial conditions for a Limited Area Model (LAM) may basically be obtained either by interpolating the initial conditions of the driving model to the LAM grid (dynamical adaptation mode) or by an independent data analysis/assimilation procedure in the LAM (data assimilation mode). The smaller the size of the LAM domain is, the more the dynamical adaptation mode is appropriate since the analysis of larger scales over a small domain becomes more and more questionable (Berre, 2000). If one wants to avoid the dilemma between the two above-mentioned basic solutions, an appropriate treatment of the larger scales may be achieved by applying a so-called blending technique where the fields of the driving model and of the LAM are selectively combined in function of the scales resolved by each model. This technique is used in ALADIN in order to keep the 4DVar ARPEGE results for the long waves, well resolved by the global model, and to combine them with the short-range meso-scale ALADIN forecast. The meso-scale part of the ALADIN solution (itself denoted as 'guess'), unresolved by ARPEGE, should thus be kept in the initial conditions. In other words the blending is a meso-scale analysis without observations, where the long-wave part of the spectra is analysed by ARPEGE and where the short-wave part of the spectra relies on its own ALADIN guess. The hypothesis is that the short-wave guess is more realistic and closer to the truth (thanks to the balance with the fine-mesh surface forcing) than the short-wave result obtained simply by interpolating the ARPEGE analysis.

The determination of the smallest scales still well captured by the analysis of ARPEGE is based on the resolution of the ARPEGE analysis increments and also on the resolution of its deterministic forecast. This scale limit, together with the size and resolution of the ALADIN domain provides a first estimate of the 'blending truncation' within the ALADIN spectra. A smooth transition between the ARPEGE and ALADIN spectra, around the blending truncation, is implicitly obtained by the Digital Filter Initialisation (DFI) method (Lynch et al., 1997). The digital filter is applied on both ARPEGE and ALADIN fields at the low spectral resolution of the blending truncation in order to obtain a filtered large-scale decrement, to be then added to the high resolution guess. The blending truncation and DFI settings are the tuning parameters of the system. The tuning criteria is to keep realistically active structures both in the initial and +6h forecasts states, together with realistic physical fluxes in the early hours of the forecast (thus taking care of the spin-up problem). Beside the smooth transition between the spectra, the digital filter offers the advantage to balance the final blending increment when adding the meso-scale ALADIN information to the large-scale part. This is ensured by the properties of the digital filter incremental initialisation, gently creating a good balance of mass and wind fields in the initial condition blended state. Any use of an external initialisation can thus be avoided.

Surface blending

DFI blending of the upper-air dynamical variables can be completed by a blending of soil variables, where the interpolation procedure transports the surface analysis increments instead of the surface analysis itself. The initial values of the surface variables in ALADIN are obtained by adding the interpolated ARPEGE surface analysis increments to the ALADIN guess. To avoid a divergence of the cycle, a weak relaxation toward the ARPEGE analysis is applied. The surface blending may easily separate the treatment of the soil and sea surfaces (a useful property in the MFSTEP case) and it can be combined with an independent surface analysis scheme (solution currently in testing phase).

2.3 NMM

2.3.1 Introduction

Within the WRF (Weather Research and Forecasting) initiative in the USA, a new approach at NCEP has been applied in developing the nonhydrostatic model NMM (Janjic et al., 2001, Janjic, 2003). Namely, instead of extending the cloud model concepts to synoptic scales and beyond, the hydrostatic approximation is relaxed in a hydrostatic model formulation. In this way the validity of the model dynamics is extended to non-hydrostatic motions, the number of prognostic equations remains the same as in the hydrostatic model, and at the same time the favorable features of the hydrostatic formulation are preserved. In high-resolution numerical weather prediction applications, the efficiency of the computational algorithm applied in the NMM significantly exceeds the efficiency of the algorithms used in several established state-of-the-art non-hydrostatic models. The high computational efficiency of the NMM has been achieved primarily due to the design of the time-stepping procedure, and due to the choice of the horizontal grid. The high computational efficiency of the NMM demonstrates that meaningful non-hydrostatic forecasting/simulations are rapidly becoming feasible at smaller centers also, using workstations and PC's. The description below is based on the Janjic (2003) article. This approach is based on relaxing the hydrostatic approximation in a hydrostatic model using vertical coordinate based on hydrostatic pressure. In this way the applicability of the model was extended to the nonhydrostatic motions. In order to do so, the system of nonhydrostatic equations was split into two parts: (a) the part that corresponds to the hydrostatic system, except for higher order corrections due to the vertical acceleration, and (b) the system of equations that allows computation of the corrections appearing in the first system due to vertical acceleration. The separation of the nonhydrostatic contributions shows in a transparent way that the hydrostatic approximation affects the equations. The described procedure does not require any linearization or approximation. At the same time, the favorable features of the hydrostatic model are preserved within the range of validity of the hydrostatic approximation. The nonhydrostatic dynamics has been introduced through an add–on module in the NCEP Meso ("Eta") model (Janjic et al., 2001). The nonhydrostatic module can be turned on and off depending on resolution. This allows easy comparison of hydrostatic and nonhydrostatic solutions obtained using otherwise identical model.

2.3.2 Governing equations

For simplicity, as a representative of mass based vertical coordinates, consider the sigma vertical coordinate

$$\sigma = \frac{(\pi - \pi_t)}{\mu}, \tag{2.3.1}$$

where π is the hydrostatic pressure, and μ represents the difference in hydrostatic pressure between the base and top of the model column; i.e.

$$\mu = \pi_s - \pi_t . \tag{2.3.2}$$

Here, π_s and π_t stand for the hydrostatic pressures at the surface and at the top of the model atmosphere. Then, the equations governing a dry, inviscid and adiabatic nonhydrostatic atmosphere are (Janjic et al., 2001)

$$\frac{\partial \mu}{\partial t} = -\int_0^1 \nabla_\sigma \bullet (\mu \mathbf{v}) d\sigma' , \tag{2.3.3}$$

$$p\alpha = RT , \tag{2.3.4}$$

$$\Phi = \Phi_s + \mu \int_\sigma^1 \frac{RT}{p} d\sigma . \tag{2.3.5}$$

$$\frac{d\mathbf{v}}{dt} = -(1+\varepsilon)\nabla_\sigma \Phi - \alpha \nabla_\sigma p + f\mathbf{k} \times \mathbf{v} , \tag{2.3.6}$$

$$\frac{\partial T}{\partial t} = -\mathbf{v} \bullet \nabla_\sigma T - \dot{\sigma}\frac{\partial T}{\partial \sigma} + \frac{\alpha}{c_p}[\mathbf{v} \bullet \nabla_\sigma p - (1+\varepsilon)\int_0^\sigma \nabla_\sigma \bullet (\mu \mathbf{v}) d\sigma'] + \frac{\alpha}{c_p}[\frac{\partial p}{\partial t} - (1+\varepsilon)\frac{\partial \pi}{\partial t}] , \tag{2.3.7}$$

$$\frac{\partial p}{\partial \pi} = 1 + \varepsilon , \tag{2.3.8}$$

$$w = \frac{1}{g}\frac{d\Phi}{dt} = \frac{1}{g}\left(\frac{\partial \Phi}{\partial t} + \mathbf{v} \bullet \nabla_\sigma \Phi + \dot{\sigma}\frac{\partial \Phi}{\partial \sigma}\right) , \tag{2.3.9}$$

$$\varepsilon = \frac{1}{g}\frac{dw}{dt} = \frac{1}{g}\Big(\frac{\partial w}{\partial t} + \mathbf{v} \bullet \nabla_\sigma w + \dot{\sigma}\frac{\partial w}{\partial \sigma}\Big). \quad (2.3.10)$$

Here, in the order of appearance, $\mathbf{v}$ is the horizontal wind vector, p is the actual, nonhydrostatic pressure, R is the gas constant for dry air, T is temperature, Φ is geopotential and Φ_S is the geopotential of the Earth's surface. The other symbols used have either their usual meaning, or their meaning is self-evident. Note that the nonhydrostatic continuity equation (2.3.9), and the definition of ε (2.3.10), are not independent equations. The parameter ε is the central point of the extended, nonhydrostatic dynamics. As can be readily verified, if ε is zero, (2.3.3)-(2.3.7) reduce to the familiar, hydrostatic equations. The additional equations (2.3.8)-(2.3.10) are needed in order to compute the corrections due to nonzero ε. On the synoptic scales, ε is small and approaches the computer round–off error. In case of vigorous convective storms, or strong vertical accelerations in the flows over steep obstacles, ε can reach the order of 10^{-3}.

2.3.3 Horizontal differencing

The NCEP/NMM and NCEP/Eta use the same type of the semi-staggered E horizontal grid. According to studies of Winninghoff (1968) and Arakawa and Lamb (1977), compared to other grids considered, generally better agreement with the exact frequencies was obtained on the staggered grid C, and on the semi-staggered grid B (or E). These considerations, however, do not give decisive advantage to either of the two choices. The problems on the semi-staggered grids B and E are restricted mainly to the shortest waves, while in the case of the slow internal modes, and/or weak stability, the C grid may develop problems in the entire range of the admissible wave numbers (Arakawa and Lamb, 1977). In addition, there is an effective technique for filtering the low frequency, short-wave noise resulting from the inaccurate computation of the divergence term on the semi-staggered grids (Janjic, 1979). More sophisticated, nondissipative methods ("deaveraging" and "isotropisation") for dealing with the problem have been also proposed (Janjic et al., 1998), leading to dramatic improvements of the finite-difference frequencies of the short gravity-inertia waves on the semi-staggered grids, particularly important for the nonhydrostatic dynamics.

2.3.4 Vertical coordinate and topography

The operational version of the NCEP hydrostatic Meso ("Eta") model uses a step-like representation of mountains originally proposed by Bryan (1969) in the z vertical coordinate. This approach was modified for a sigma coordinate model by Mesinger et al. (1988). The advantage of the step-like mountain representation is that the coordinate surfaces are quasi-horizontal. This, however, is not without consequences. For example, internal discontinuities are introduced at the vertical sides of the steps that replace the mountain slopes, and lateral boundary conditions are required at these discontinuities. The formal accuracy of the finite-differences at the points next to the internal boundaries is reduced to the first order. In addition to that, if the no slip boundary conditions are used in order to preserve in a simple way the major favorable features of the finite-differencing schemes (Janjic, 1977, 1979, 1984), a nonphysical sink of momentum is introduced. Yet another problem is the representation of the physical processes in the surface layer and the planetary boundary layer (PBL). The vertical resolution needed for adequate treatment of the PBL should be rather fine. This was one of the major problems in the process of developing the physical package for the Meso ("Eta") model (Janjic, 1990, 1994). However, with the increasing computing power and model resolutions, several problems that could be associated with the step-mountain representation of topography started to surface up, particularly at smaller scales, and in mountainous areas. For example, the model using the step-mountain representation failed to reproduce a catabatic windstorm in the Rockies, while the forecast using the conventional sigma coordinate was quite successful in this respect (Janjic and DiMego, 2001). In addition, several recent studies (Adcroft et al, 1997; Galus, 2000, Gallus and Klemp, 2000, Janjic and DiMego, 2001) indicate that more problems should be expected at even higher resolutions. Another problem possibly related to the mountain representation is that the NCEP operational Meso model using the step-mountains is producing precipitation too far down on the slopes of major orographic obstacles (Staudenmeier and Mittelstadt, 1998). In response to the step-mountain problems, in the nonhydrostatic Meso model the conventional σ coordinate terrain-following representation of mountains has been used in most tests so far. Recently, the hybrid pressure-sigma vertical coordinate option has been introduced (Arakawa and Lamb, 1977). With the hybrid coordinate, the coordinate surfaces are flat above and away from the mountains. In the vicinity of the mountains the hybrid coordinate has increased vertical resolution, and the equations are continuous, without the computational internal boundary conditions that have to be specified with the step-mountains. The sloping coordinate surfaces in the vicinity of the mountains, and the related inaccuracies, are the price to pay for these benefits. The usual, Lorenz vertical staggering of the variables is used in the vertical. The geopotential and the nonhydrostatic pressure are defined at the interfaces of the layers, while all three velocity components and temperature are carried in the middle of the model layers. The vertical velocity is defined at the E grid mass points.

2.3.5 Time differencing

In the NCEP hydrostatic Meso ("Eta") model additive time splitting is used. The hydrostatic system of equations is split into the following two subsystems

$$\left(\frac{\partial \mathbf{v}}{\partial t}\right)_i = -\nabla_\sigma \Phi - \alpha \nabla_\sigma \pi + f\mathbf{k}\times\mathbf{v} \tag{2.3.11}$$

$$\left(\frac{\partial T}{\partial t}\right)_i = \frac{\alpha}{c_p}[\mathbf{v}\cdot\nabla_\sigma \pi - \int_0^\sigma \nabla_\sigma \cdot (\mu\mathbf{v})\, d\sigma'] \tag{2.3.12}$$

$$\left(\frac{\partial \mu}{\partial t}\right)_i + \nabla_\sigma \cdot (\mu\mathbf{v}) + \frac{\partial(\mu\dot{\sigma})}{\partial\sigma} = 0 \tag{2.3.13}$$

$$\left(\frac{\partial \mathbf{v}}{\partial t}\right)_{ii} = -\mathbf{v}\nabla_\sigma \mathbf{v} - \dot{\sigma}\frac{\partial \mathbf{v}}{\partial \sigma} \tag{2.3.14}$$

$$\left(\frac{\partial T}{\partial t}\right)_{ii} = -\mathbf{v}\cdot\nabla_\sigma T - \dot{\sigma}\frac{\partial T}{\partial \sigma} \tag{2.3.15}$$

The time derivatives of the two subsystems are denoted by subscripts *i* and *ii*, respectively. The system (2.3.11)-(2.3.13) is solved using short time steps, and the system (2.3.14)-(2.3.15) is solved using long time steps. The system (2.3.11)–(2.3.13) conserves energy. The system (2.3.14)–(2.3.15) also conserves energy, except for the changes due to the redistribution of mass. An economical forward–backward scheme (Ames, 1969; Gadd, 1974) with the trapezoidal scheme for the Coriolis term (Janjic and Wiin–Nielsen, 1977) has been used for the system (2.3.11)–(2.3.13) (Janjic, 1979). Concerning the contributions of the advection terms (2.3.14)–(2.3.15), the two–step iterative Adams–Bashforth scheme is used. The Adams–Bashforth scheme allows about the same computational efficiency as the two–step, iterative scheme with twice longer time steps. The Adams-Bashforth scheme has also been used for the Coriolis force terms. Another recent novelty is that the iterative method for solving the vertical implicit pressure equation discussed in Janjic et al. (2001) has been replaced by direct solver. This modification has brought a visible improvement in the computational efficiency of the model.

3 SVP Hindcasts

In the framework of the SVP of WP10, IASA, CHMI and ICoD performed high-resolution (0.1°x0.1°) hindcast simulations using the nonhydrostatic SKIRON/Eta, ALADIN and NCEP/NMM models, respectively. The SKIRON/Eta and Aladin atmospheric limited area models produced 72-hour hindcasts initialized from the daily 0000 UTC ARPEGE analyses of January 2003. NMM/NCEP model also utilized the same initial and lateral boundary conditions, but it produced hindcasts up to 24 hours. The ARPEGE fields had been provided by Meteo-France at a resolution of 0.25 x 0.25 degrees.

In SKIRON/Eta the initialization of the soil moisture and temperature was performed using the 24-hour forecast of the run of the previous day. In Aladin model the assimilation mode started one day prior to the SVP, i.e. 31/12/2002 00 UTC in order to avoid spin-up of the assimilation cycle. This was based on the late cut-off time of the 4DVAR data assimilation system of the global model ARPEGE. Every day at 00 UTC a +72h forecast has been run, where initial files were obtained from the Aladin/Mfstep assimilation cycle, and the lateral boundary data were provided by the early cut-off forecasts of the driving model ARPEGE.

The computational domain of all models covered the whole Mediterranean region and part of Central Europe (Figures 1, 2). Following the decisions made at the WP10 meeting in Athens, the subtask partners decided that both SKIRON/Eta and Aladin models would provide forecasts for the whole Mediterranean and Black sea regions. Therefore the dissemination domain of SKIRON/Eta model extended from 29°N to 48°N and from 11°W to 42°E (Figure 1). The Aladin raw data were post-processed separately on two domains (Mediterranean = 30°N-48°N, 19°W-37°E; Black-Sea = 40°N-48°N, 27°E-42°E; see Figure 2). The verification domain of NMM was identical to that of SKIRON/Eta (29°N-48°N, 11°W-42°E). The output fields were available every hour at a horizontal grid of 0.1x0.1 degrees.

The SKIRON/Eta and ALADIN-MFSTEP meteorological fields that became available to the project partners (hourly) in GRIB format were the u and v component of the 10m. wind, the 2m. air temperature, the 2m. specific humidity, the cloud fraction, the mean sea-level pressure (MSLP), the total accumulated precipitation, the downward/upward shortwave and longwave radiative fluxes, the evaporation, the surface latent and sensible heat flux, the land-sea mask and the sea-surface temperature. Moreover, ALADIN provided the same radiation fluxes but computed for a cloudless atmosphere. In addition to the required surface variables, SKIRON/Eta, Aladin and NMM delivered (to the partners of subtask 10510) the upper air fields of geopotential, temperature, humidity and wind components at 500 and 850 hPa every 6 hours for the purpose of the model validation and inter-comparison.

More detailed information about the SVP hindcasts and their availability can be found in the deliverables 6 and 7 of MFSTEP-WP10.

4 Methods for model Inter-comparison and Validation

The statistical analysis exhibits some differences depending on whether the meteorological variables are discrete or continuous. Discrete variables are allowed to take on only a finite number of values, whereas continuous variables may take on any of the infinitely many real values within their range. The rainfall, snowfall and the cloud cover are considered to be discrete variables, while the temperature, the wind speed and the mean sea-level pressure are continuous variables. On the surface of the earth, the forecasts and the observations of continuous meteorological variables result from a finite number of discrete values.

The statistical methods that were applied to the examined continuous variables were the bias (BIAS) and the root mean square error (RMSE).

Bias (BIAS):

The bias estimates the correspondence between the mean value of the forecast (F) and the observation (O). This measure calculates the sum of the differences in a total of N values:

$$BIAS = \frac{1}{N}\sum_{i=1}^{N}(F_i - O_i) = \overline{F} - \overline{O}$$

If $BIAS<0$ (>0), the model underestimates (overestimates) the specific variables.

Root Mean Square Error (RMSE):

This measure is considered to be one of the most popular in the estimation of the forecast accuracy (Wilks, 1995; Katsafados, 2003 and others). It is mostly used in grid-point fields and it is expressed by:

$$RMSE = \sqrt{\frac{1}{N}\sum_{i=1}^{N}(F_i - O_i)^2}$$

RMSE takes values greater than or equal to zero. This value is not dimensionless but it exhibits the same units as the validated field. It is an important measure as it provides a quantitative measure of the model performance.

5 Statistical analysis

The statistical analysis was mainly based on the SVP hindcasts performed by SKIRON/Eta, Aladin/MFSTEP and NMM models. The examined surface fields are the mean sea-level pressure, the 2m temperature and the 10m wind speed, while the examined upper-air fields are the geopotential height, the temperature, the specific humidity and the U and V wind components. All the upper-air fields were evaluated at 500 and 850 mb. These are the most suitable levels for evaluating the upper-air forecasts because the geopotential height at 500 mb is usually used to examine the large-to-synoptic scale circulation while the isobaric level of 850 mb is suitable for the investigation of temperature advection. The data used for validation purpose were 6-hourly MF and ECMWF analyses (GRIB format, 0.25°x0.25° and 0.5°x0.5° respectively) for upper-air parameters and 6-hourly ECMWF analyses (GRIB format, 0.5°x0.5°) for surface parameters. All analysis and forecast data sets were firstly interpolated into a 0.1°x 0.1° grid over the verification area of each model.

5.1 SKIRON/Eta

5.1.1 Verification during SVP

The verification statistics of SKIRON/Eta model exhibit a good agreement against MF and ECMWF gridded analyses. The geopotential height at 500 mb was usually underestimated and its RMSE was less than 20 gpm in the first two forecast days while it increased up to about 30 gpm at T+72 hours (Figure 3). On the other hand, the geopotential height at 850 mb was usually overestimated and the RMSE reached 21 gpm at the end of the forecast period (Figure 4). The temperature at 500 mb and 850 mb was slightly underestimated, with the absolute value of the bias being smaller than 1°C at both levels (Figures 5, 6). The RMSE of temperature at 500 mb increased from about 0.6°C at T+6 to about 1.7-1.8°C at T+72. Similarly, the RMSE of temperature at 850 mb ranged from about 1.1°C in the beginning of the forecast period to 1.9°C at T+72.

At the surface, the RMSE of 10m wind speed and 2m temperature increased slightly during the forecast period, while the same error of the MSLP exhibited a gradual increase

(Figure 7). The RMSE of 10m wind speed was between 2 and 2.3 m/s and that of 2m temperature was between 1.6 and 2.6°C. The 10m wind speed was overestimated having a maximum bias of 0.4 m/s (Figure 7a). The bias of 2m temperature and MSLP were in qualitative agreement since the former field was underestimated while the latter one was generally overestimated (Figures 7b, c).

The above results indicate that the model was consistent throughout the forecast period and the increase of the errors was relatively small during the runs. This is obvious in the near-surface fields of 10m wind speed and 2m temperature. Similarly, the RMSE of the temperature at 850 mb and 500 mb increased by 0.8°C and 1.2°C, respectively, from T+6 to T+72. Finally, it appears that the differences of the statistical scores are negligible when the upper-air forecasts are compared to gridded analyses from different centers (MF or ECMWF).

(a)

(b)

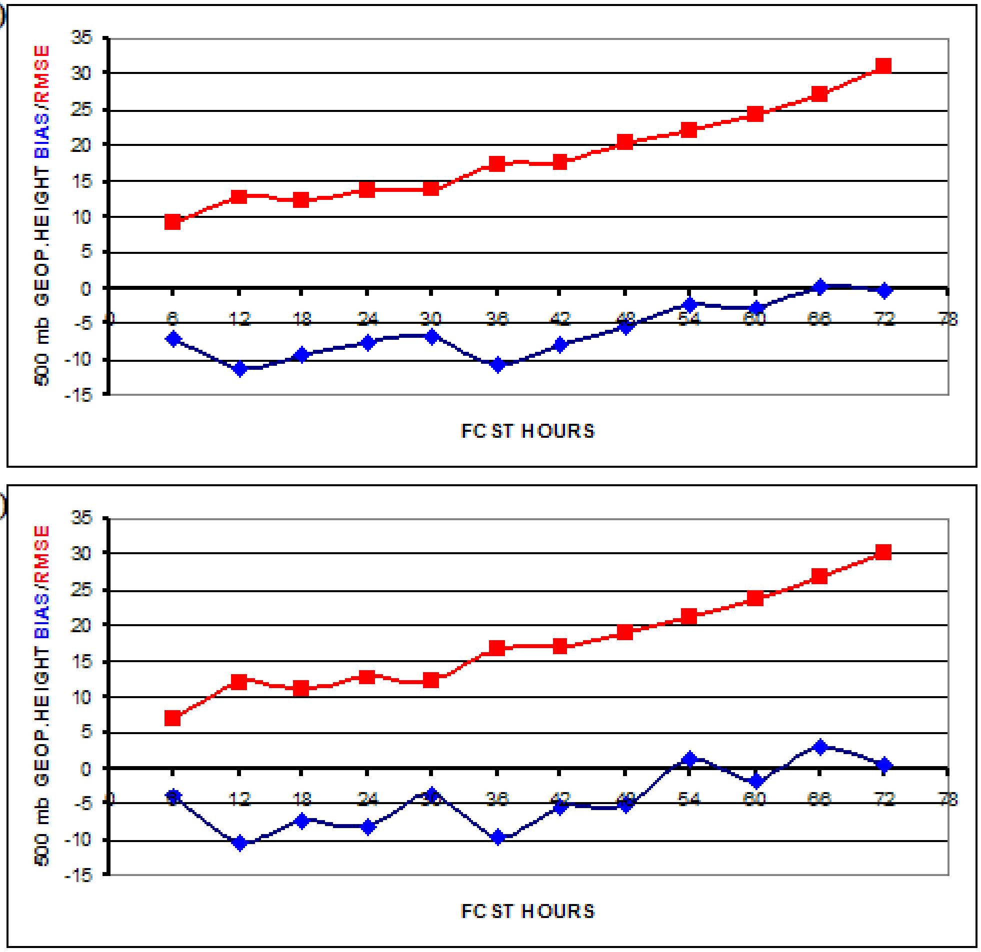

Figure 3. *Bias (blue line) and RMSE (red line) of the 500 mb geopotential height (gpm) forecasts of SKIRON/Eta in SVP period using a) MF and b) ECMWF gridded analyses.*

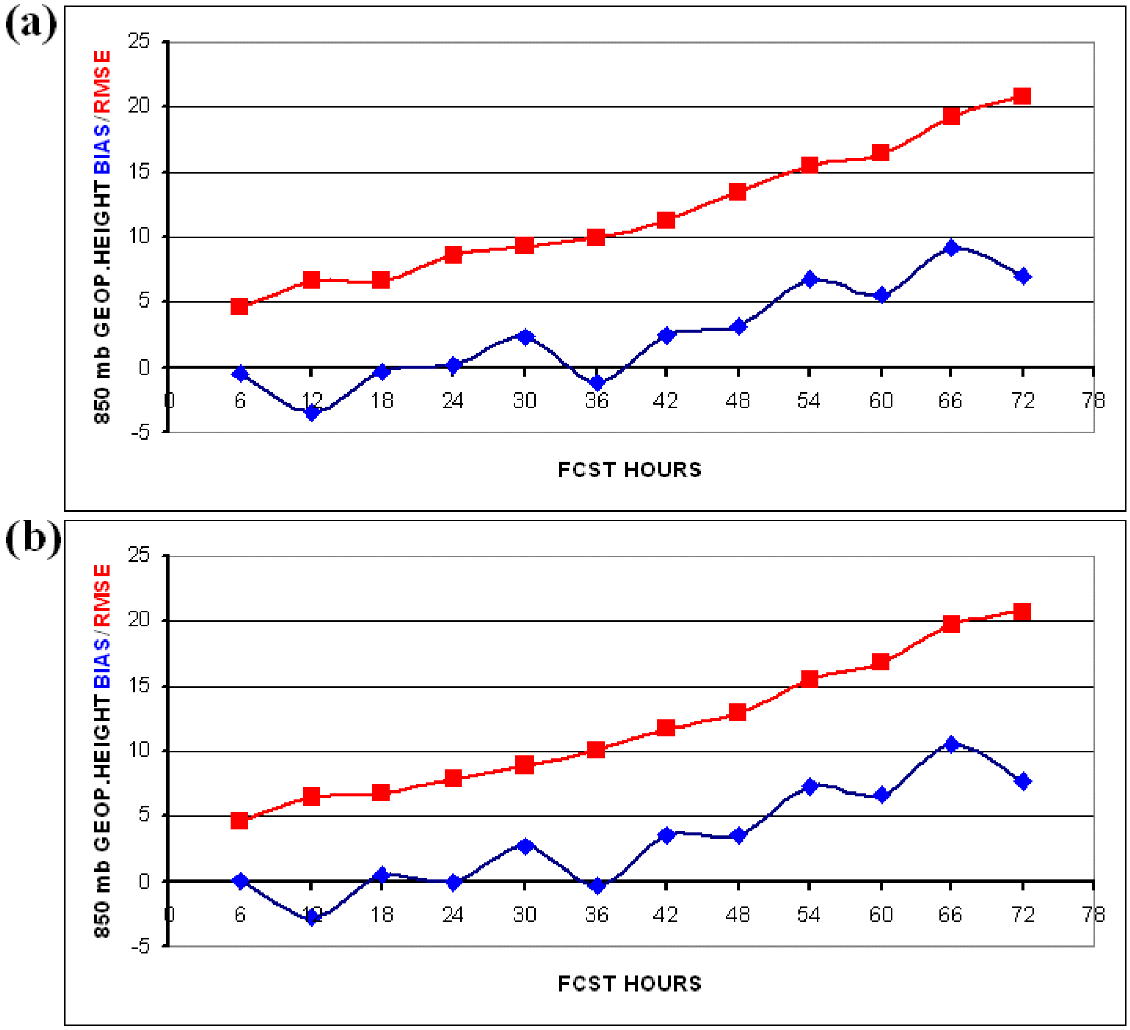

Figure 4. *Bias (blue line) and RMSE (red line) of the 850 mb geopotential height (gpm) forecasts of SKIRON/Eta in SVP period using a) MF and b) ECMWF gridded analyses.*

(a)

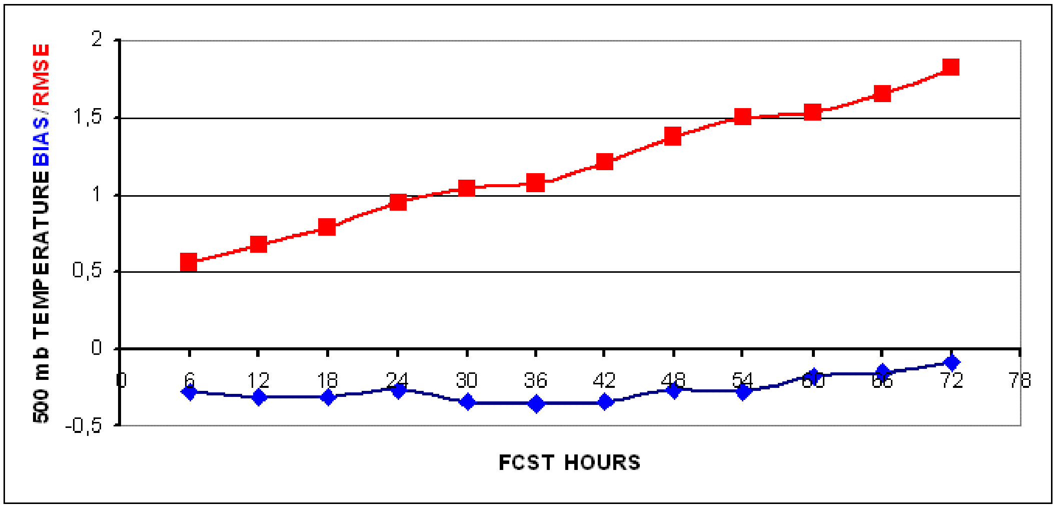

(b)

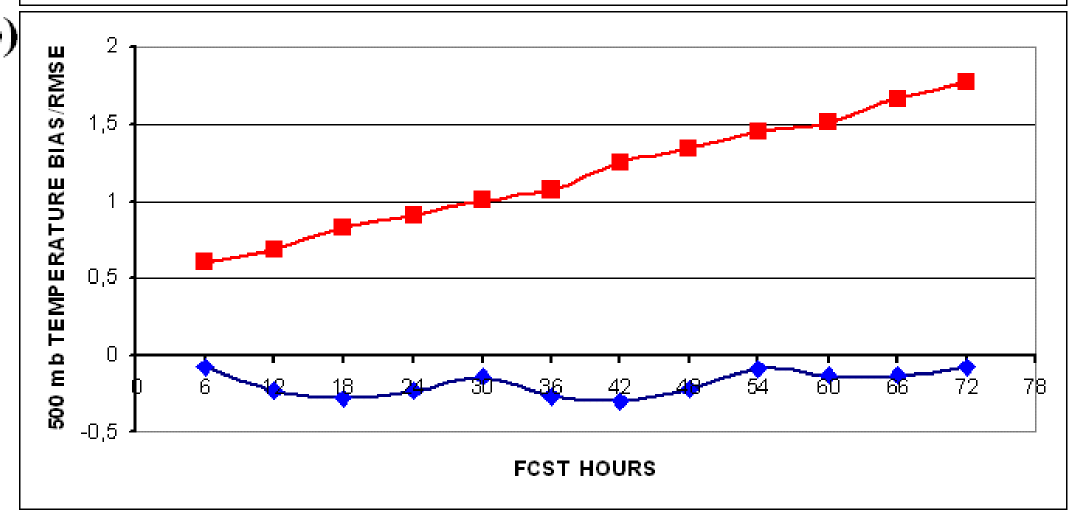

Figure 5. *Bias (blue line) and RMSE (red line) of the 500 mb temperature (℃) forecasts of SKIRON/Eta in SVP period using a) MF and b) ECMWF gridded analyses.*

(a)

(b)

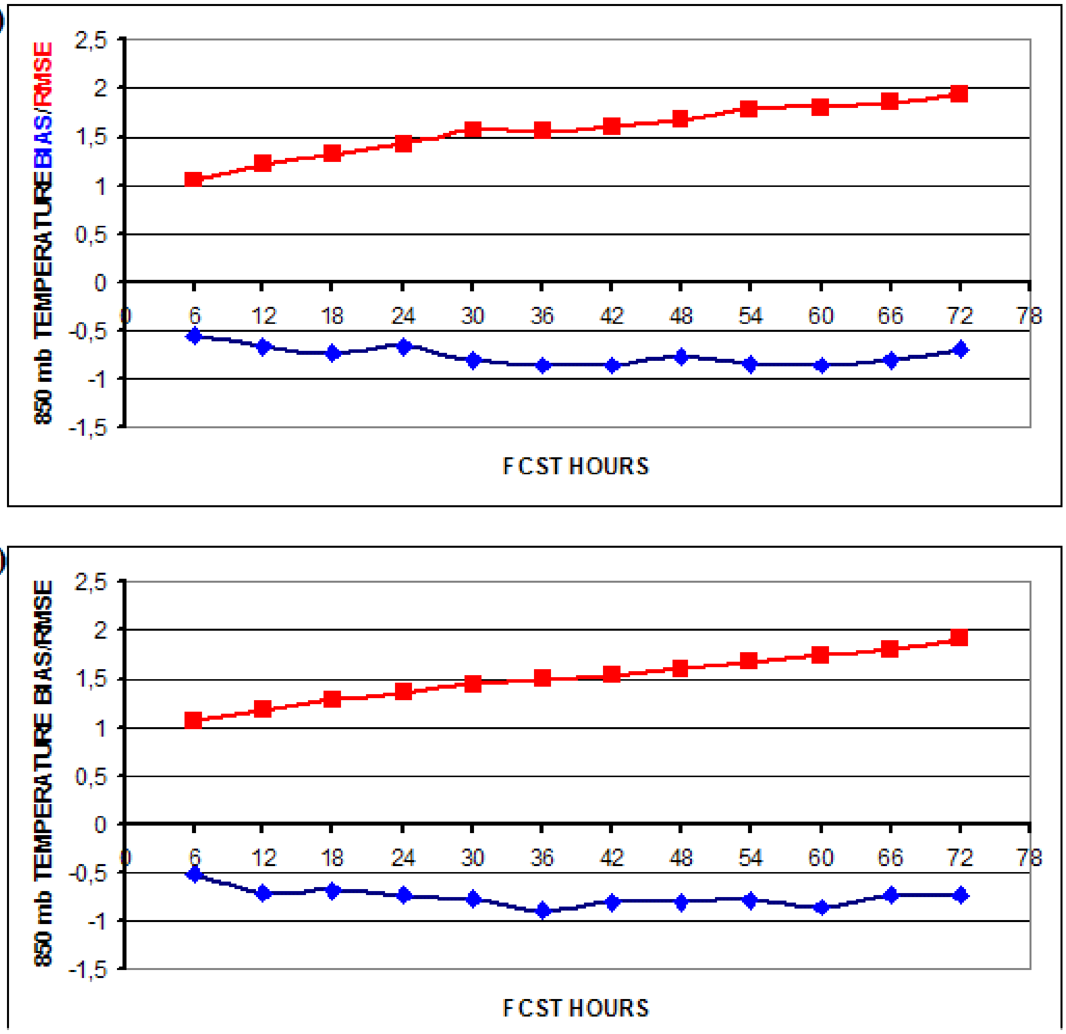

Figure 6. *Bias (blue line) and RMSE (red line) of the 850 mb temperature (°C) forecasts of SKIRON/Eta in SVP period using a) MF and b) ECMWF gridded analyses.*

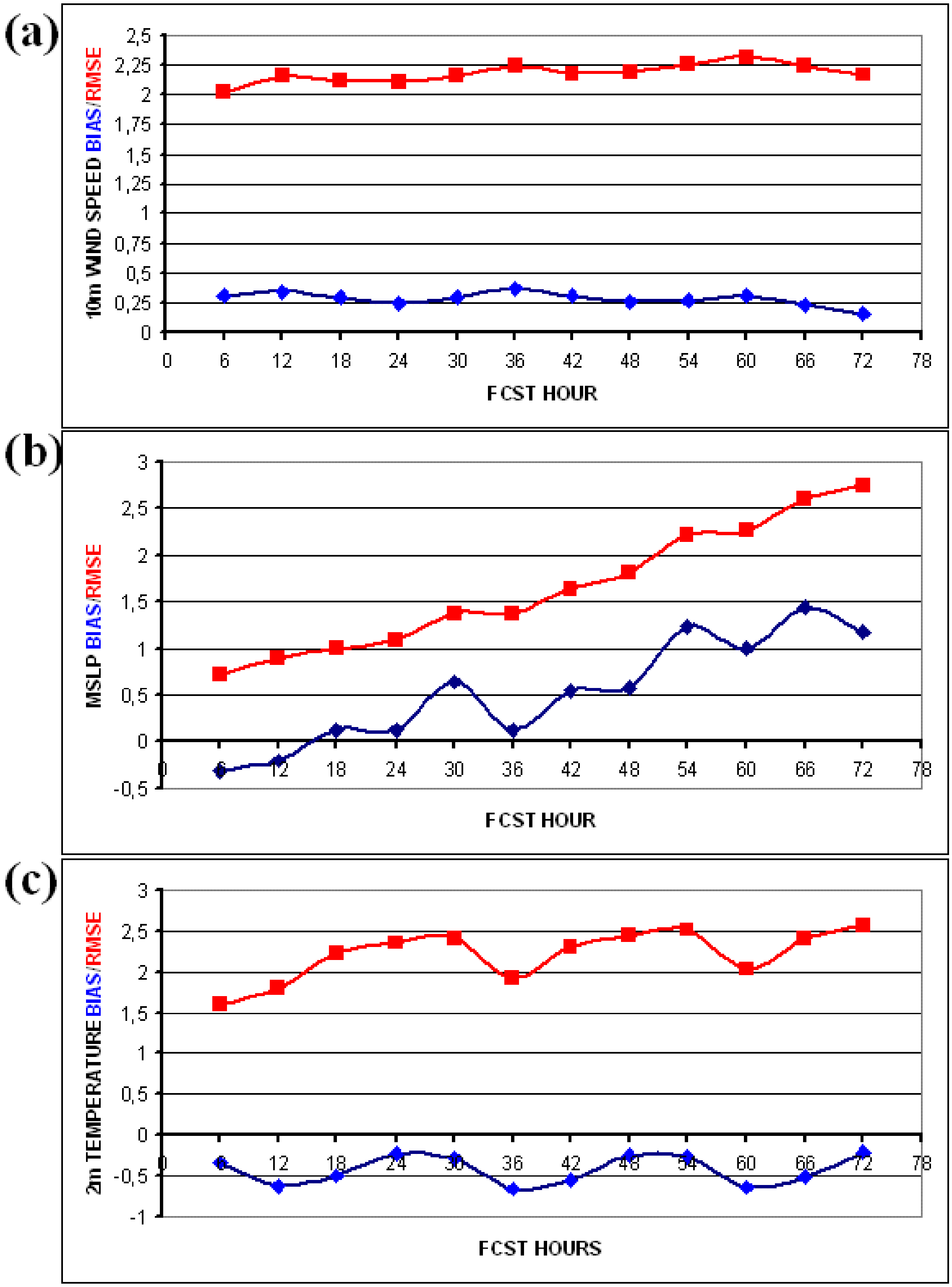

Figure 7. *Bias (blue line) and RMSE (red line) of the SKIRON/Eta SVP forecasts of a) 10m wind speed (m/s), b) MSLP (hPa) and c) 2m Temperature (℃) using ECMWF gridded analyses.*

5.1.2 Verification against buoys for 2004-2005

SKIRON/Eta model was also verified using a number of available buoy observations in the Aegean sea. These forecasts were produced by the operational SKIRON/Eta model that provides 5-day forecasts for the Mediterranean and Black sea region on a daily basis. These predictions are not produced in the framework of MFSTEP project, but they are operationally available to all the MFSTEP partners. The computational and dissemination domains are identical to those used during TOP. More information can be found in the Final scientific reports of the MFSTEP subtasks 10140 and 10520.

The available buoy data covered the period from January 2004 to September 2005. Their locations appear in Table 1.

Location	Latitude (°N)	Longitude (°E)
Athos	39.963	24.724
Augo	35.62	25.641
Aegina	37.827	23.472
Lesvos	39.15	25.809
Mykonos	37.511	25.454
Santorini	36.254	25.492

Table 1: *Coordinates of the available buoys in the Aegean sea.*

Figure 8 presents a scatter plot of the SKIRON/Eta forecasts against observations of the wind speed at the locations of all the available buoys, while Figures 9-11 present the Bias, RMSE and correlation coefficient at the location of each buoy. The correlation coefficient is an indication of the relationship between the values of two variables and it is defined as the ratio of the covariance of the values of two populations relative to the product of their standard deviations:

$$r_{F,O} = \frac{\mathrm{cov}(F,O)}{s_F \cdot s_0}$$

This statistical measure is calculated using the following formula:

$$r_{F,O} = \frac{1}{N-1}\sum_{i=1}^{N}\left[\frac{(F_i - \overline{F})}{s_F}\frac{(O_i - \overline{O})}{s_O}\right] = \frac{\sum_{i=1}^{N}(F_i O_i) - \frac{1}{N}\left[\sum_{i=1}^{N}(F_i)\right]\left[\sum_{i=1}^{N}(O_i)\right]}{\sqrt{\left[\sum_{i=1}^{N}F_i^{\,2} - \frac{1}{N}\left(\sum_{i=1}^{N}F_i\right)^2\right]\left[\sum_{i=1}^{N}O_i^{\,2} - \frac{1}{N}\left(\sum_{i=1}^{N}O_i\right)^2\right]}}$$

where $s_X = \sqrt{\frac{1}{N-1}\sum_{i=1}^{N}(X_i - \overline{X})^2}$ is the standard deviation of the variable X.

The correlation coefficient takes values between -1 and 1 (included). $r_{F,O} = -1$ indicates the existence of anticorrelation between the two populations, while $r_{F,O} = +1$ indicates a perfect correlation. Values of $r_{F,O}$ equal to zero indicate that the two populations are not correlated.

These diagrams show that SKIRON/Eta exhibit a very good forecast skill. Regarding the buoy of Aegina, the errors are mainly due to its location (proximity of land around it). On the other hand, very good predictions appear in the locations of Avgo, Athos and Mykonos.

In the validation of the model predictions, one must consider that the model resolution is not adequate for the prediction of near-surface parameters in closed coastal regions. The nearby islands, especially in southern Aegean sea, necessitate the use of a better horizontal resolution. This was achieved in the experiments of MFSTEP subtask 10410 in which a horizontal grid-increment of 5 km was used. However, the operational use of such a high horizontal resolution is not feasible at the moment due to large computational cost. Another source of systematic errors is the interpolation method. Finally, it needs to be pointed out that this kind of statistical evaluation is strongly dependent on the observational errors. The locations of the observing systems, such as the buoys, are not always the most suitable since they are close to coastal areas. This influences the buoy measurements and therefore their reliability.

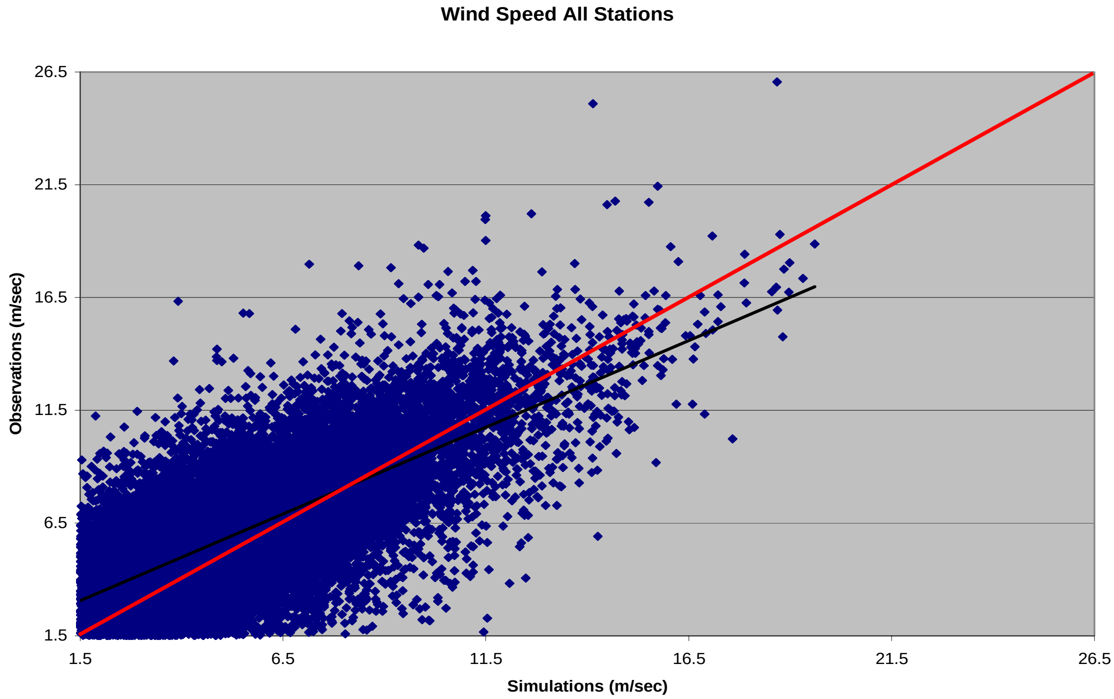

Figure 8. *Scatter plot of SKIRON/Eta forecasts against observations of the wind speed for all the available buoys. The red line shows the optimum model performance and the black line shows the best fit of the model forecasts.*

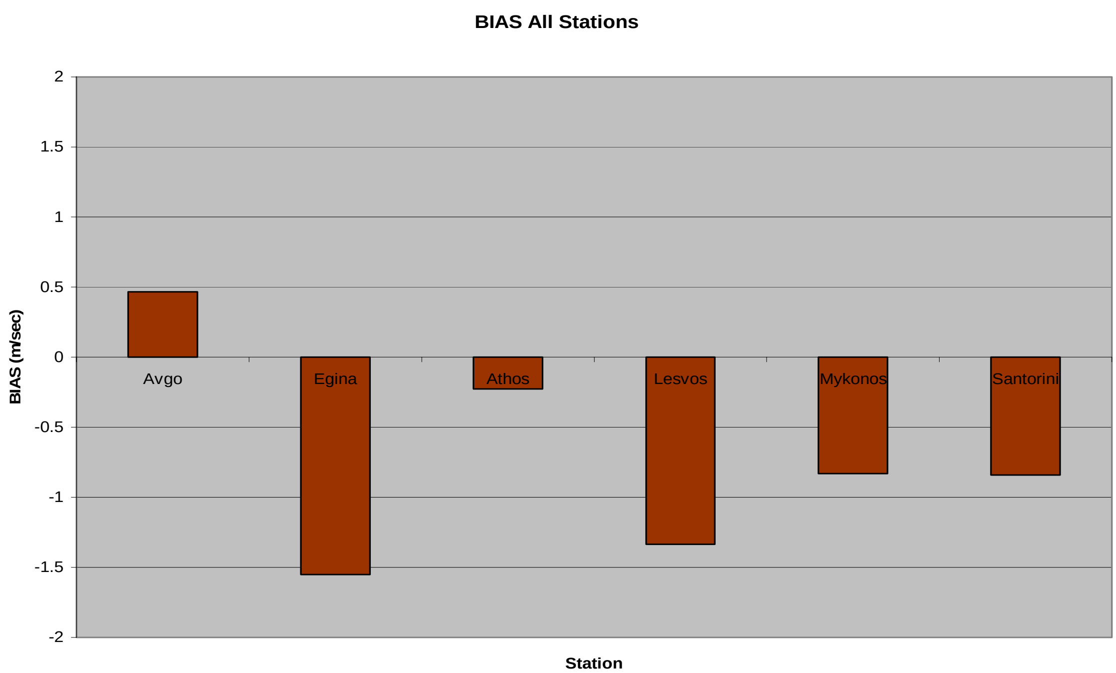

Figure 9. *BIAS of SKIRON/Eta wind speed (m/s) forecasts at the location of each available buoy.*

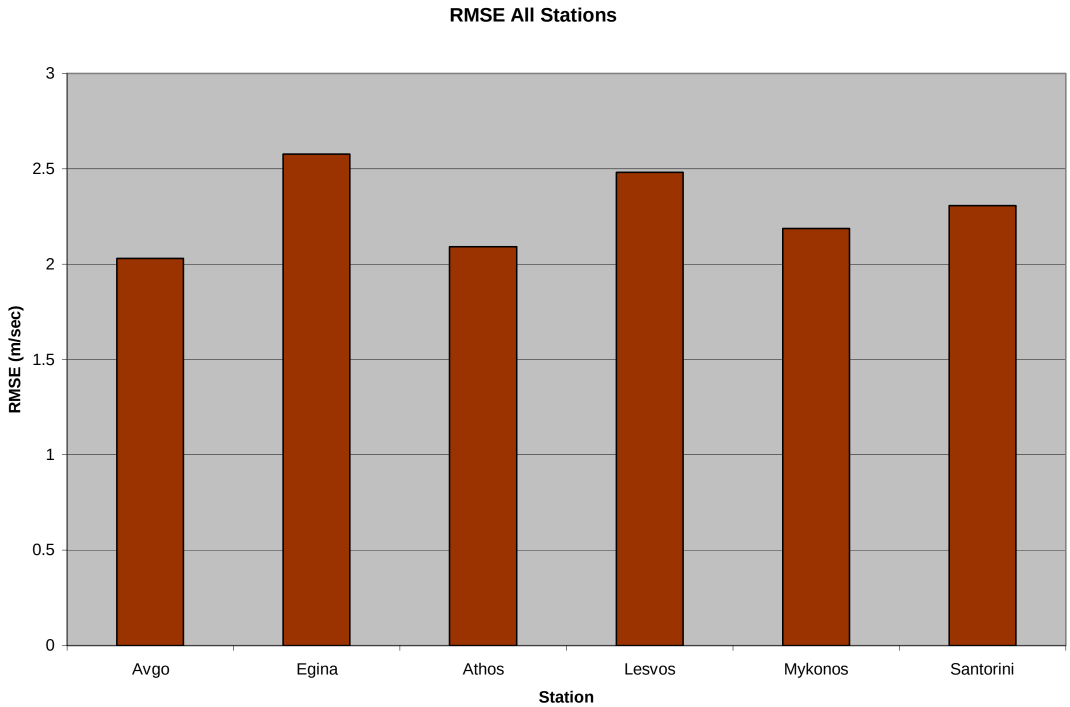

Figure 10. *RMSE of SKIRON/Eta wind speed (m/s) forecasts at the location of each available buoy.*

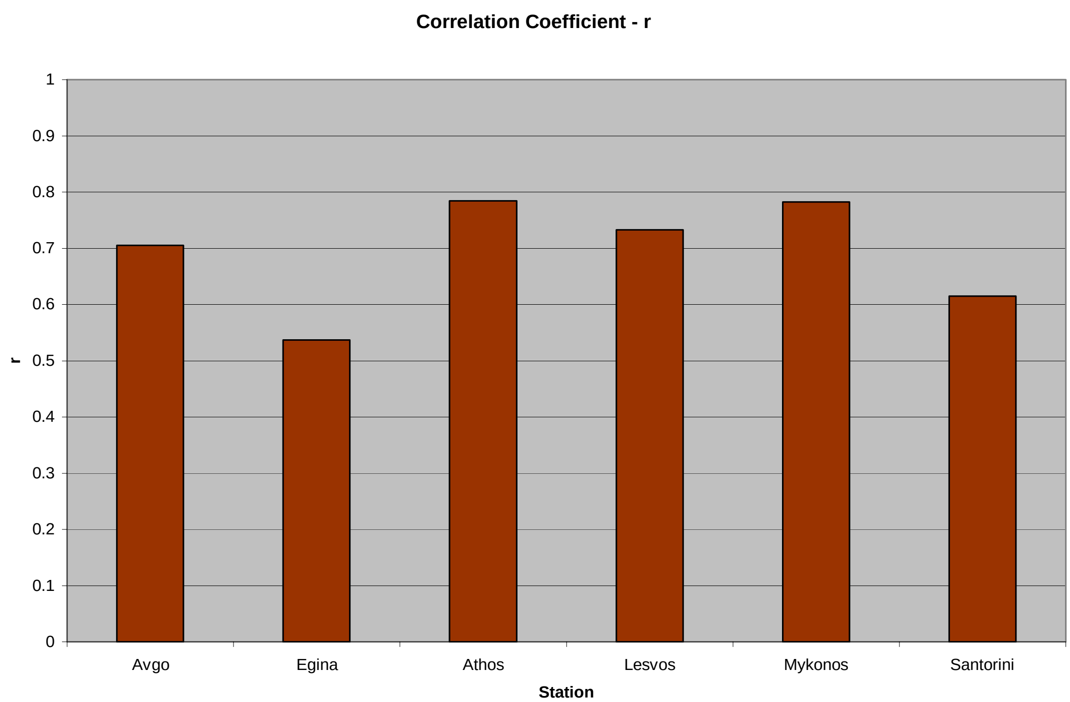

Figure 11. *Correlation coeeficient (r) of SKIRON/Eta wind speed forecasts at the location of each available buoy.*

5.2 Aladin/MFSTEP

The verification statistics of Aladin/MFSTEP model were calculated in both dissemination domains of the Mediterranean sea and the Black sea (see Figure 2). The skill scores exhibited a good agreement against MF and ECMWF gridded analyses. The geopotential height at 500 mb was usually overestimated over the Mediterranean region and its RMSE was less than 20 gpm up to about T+48 while it increased up to about 34 gpm at T+72 hours (Figure 12). The geopotential height at 850 mb over the Mediterranean was also overestimated (mainly in the 3rd forecast day) and the RMSE reached 22 gpm at the end of the forecast period (Figure 13). The temperature at 500 mb and 850 mb were underestimated and overestimated (respectively), with the absolute value of the bias being smaller than 0.7°C at both levels (Figures 14, 15). In agreement with SKIRON, the RMSE of temperature at 500 mb increased from about 0.6°C at T+6 to about 1.9°C at T+72 and the RMSE of temperature at 850 mb ranged from about 0.9-1°C in the beginning of the forecast period to 1.8°C at T+72.

In the Mediterranean region, the RMSE of 10m wind speed and 2m temperature increased slightly during the forecast period, while the same error of the MSLP exhibited a gradual increase (Figure 16). The RMSE of 10m wind speed was between 2 and 2.4 m/s and that of 2m temperature was between 1.6 and 2.7°C. The 10m wind speed was overestimated having a maximum bias of 0.3 m/s (Figure 16a). The 2m temperature did not exhibit a clear bias while the MSLP was clearly overestimated only during the 3rd forecast day (Figures 16b, c).

The skill scores over the Black sea (Figures 17-21) were in general agreement with those over the Mediterranean sea region. The most important difference appeared in the scores of the near-surface fields. More specifically, the MSLP was systematically underestimated with a maximum bias of -1 mb (Figure 21b), while the 2m temperature was systematically overestimated with a maximum bias up to about 1°C (Figure 21c). Moreover, the forecasts of 850 mb temperature over the Black sea exhibited a larger RMSE and a systematic larger increase of bias than over the Mediterranean sea region (Figures 15, 20). This may be indicative of a potential weakness of the model to analyze accurately either the cold intrusions that occur in the Black sea during winter and bring very cold air-masses (usually of Siberian origin) over eastern Mediterranean or the southwesterly flow that was very frequent in this region during January 2003.

The above results indicate that the model was consistent throughout the forecast period and the increase of the errors was relatively small during the runs. This occurs mainly in the near-surface fields of 10m wind speed and 2m temperature. Special attention is given to the model predictions near the surface because the surface fields were used by the wave and ocean models of the MFSTEP project. Moreover, it appears that the differences of the statistical scores are negligible when the upper-air forecasts are compared to gridded analyses from different centers (MF or ECMWF).

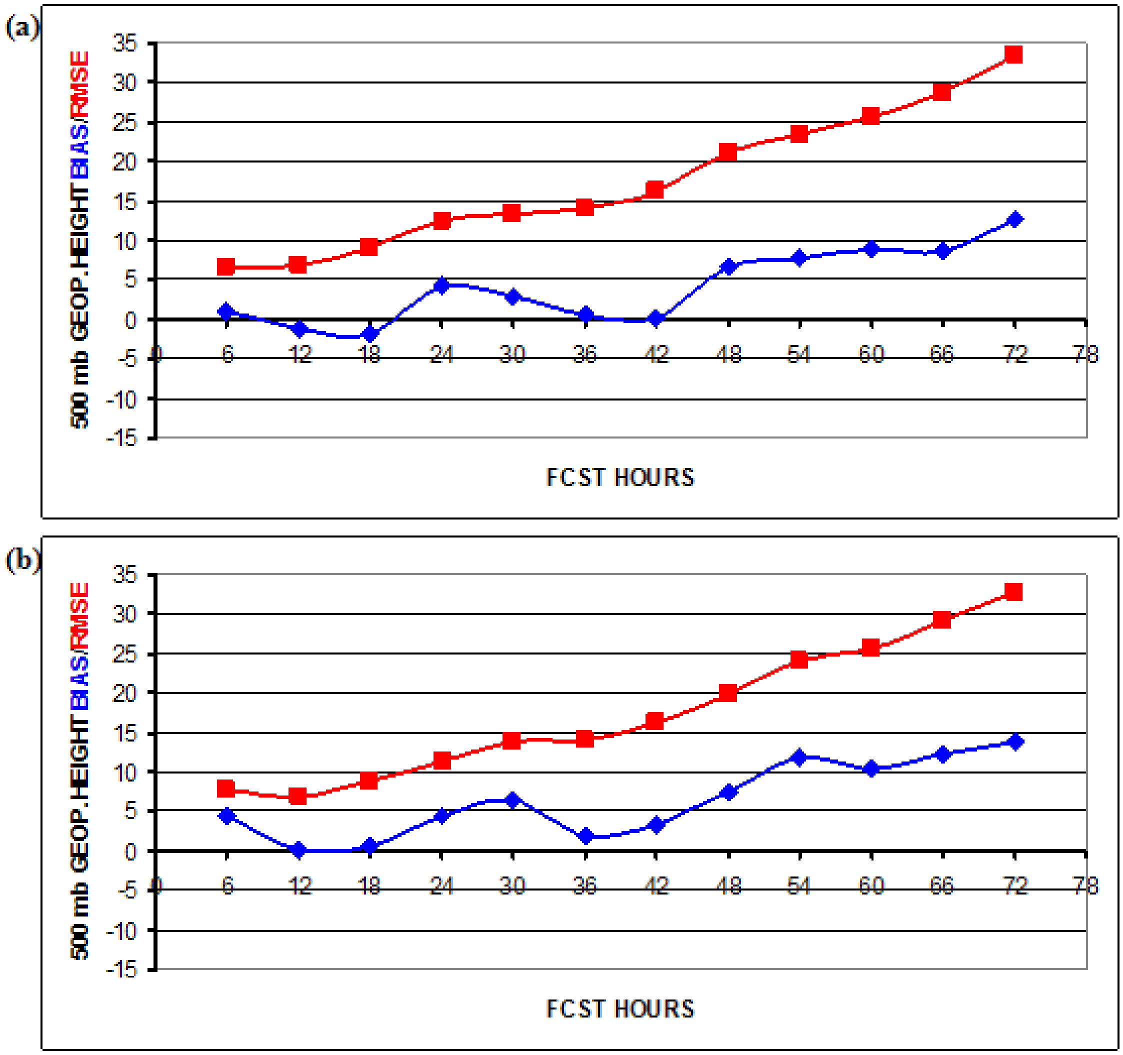

Figure 12. *Bias (blue line) and RMSE (red line) of the 500 mb geopotential height (gpm) forecasts of Aladin/MFSTEP in the Mediterranean sea region in SVP period using a) MF and b) ECMWF gridded analyses.*

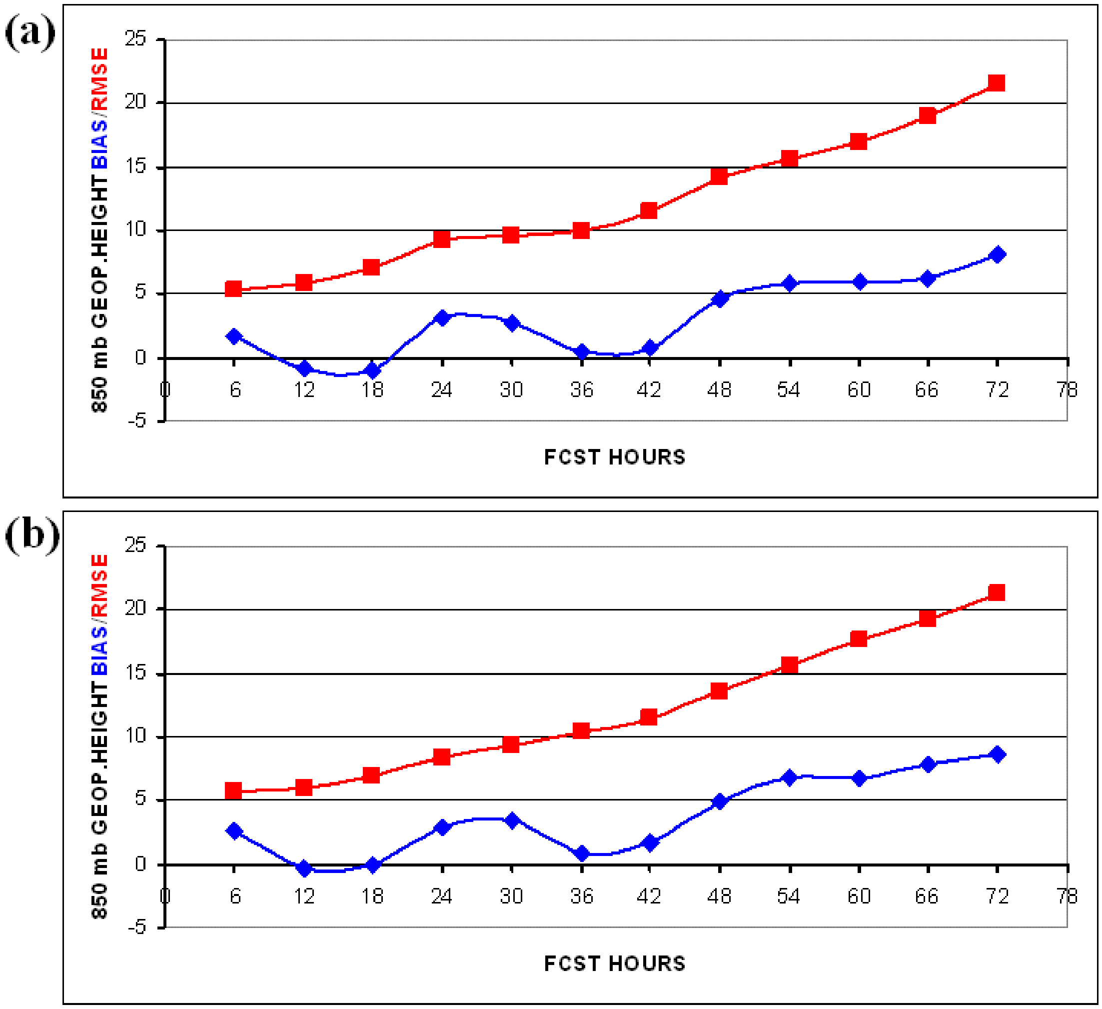

Figure 13. *Bias (blue line) and RMSE (red line) of the 850 mb geopotential height (gpm) forecasts of Aladin/MFSTEP in the Mediterranean sea region in SVP period using a) MF and b) ECMWF gridded analyses.*

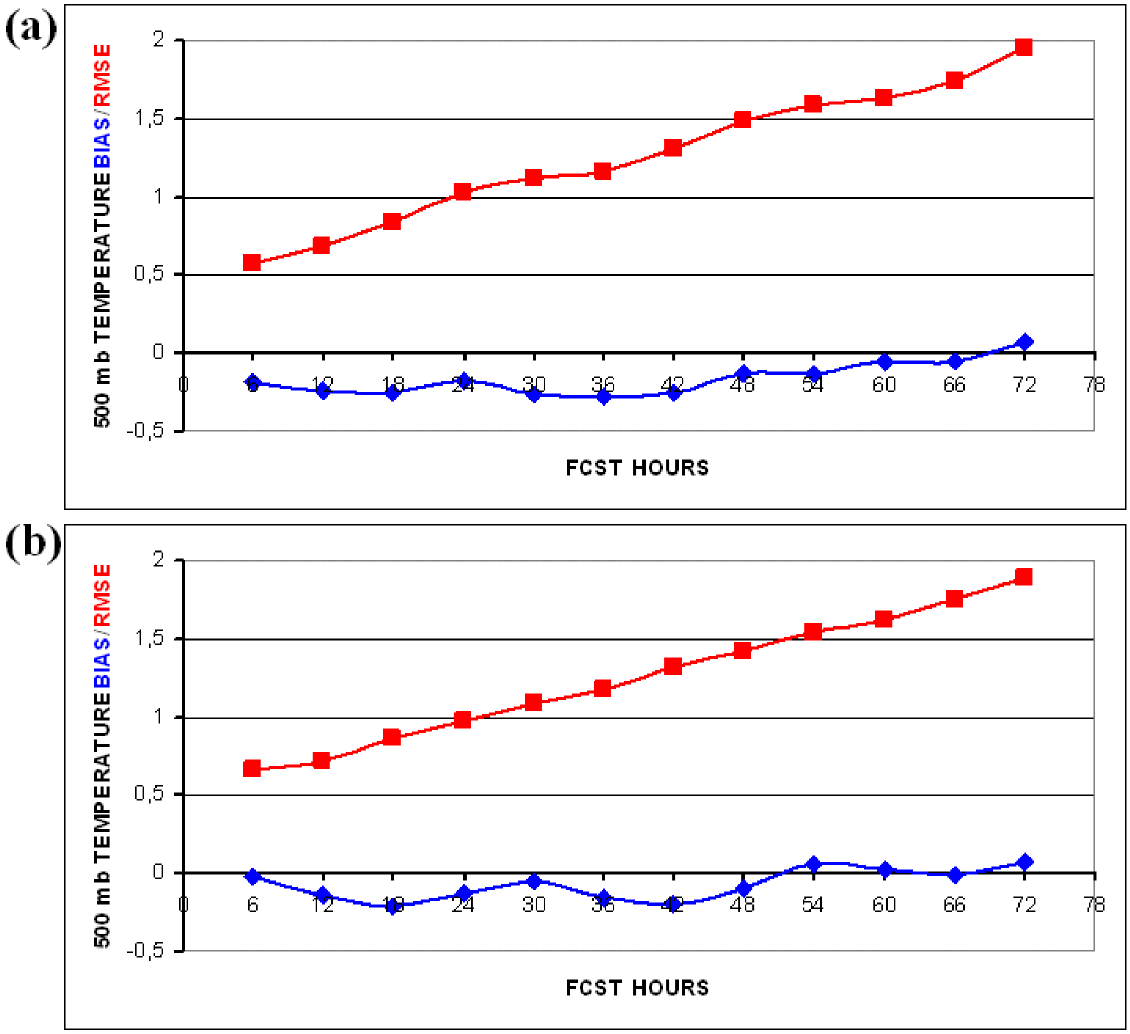

Figure 14. *Bias (blue line) and RMSE (red line) of the 500 mb temperature (℃) forecasts of Aladin/MFSTEP in the Mediterranean sea region in SVP period using a) MF and b) ECMWF gridded analyses.*

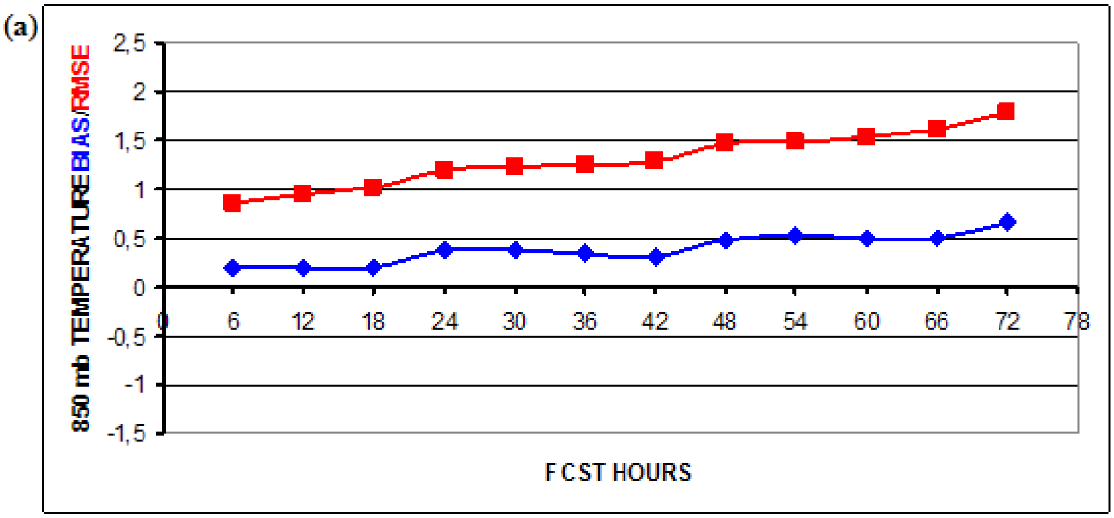

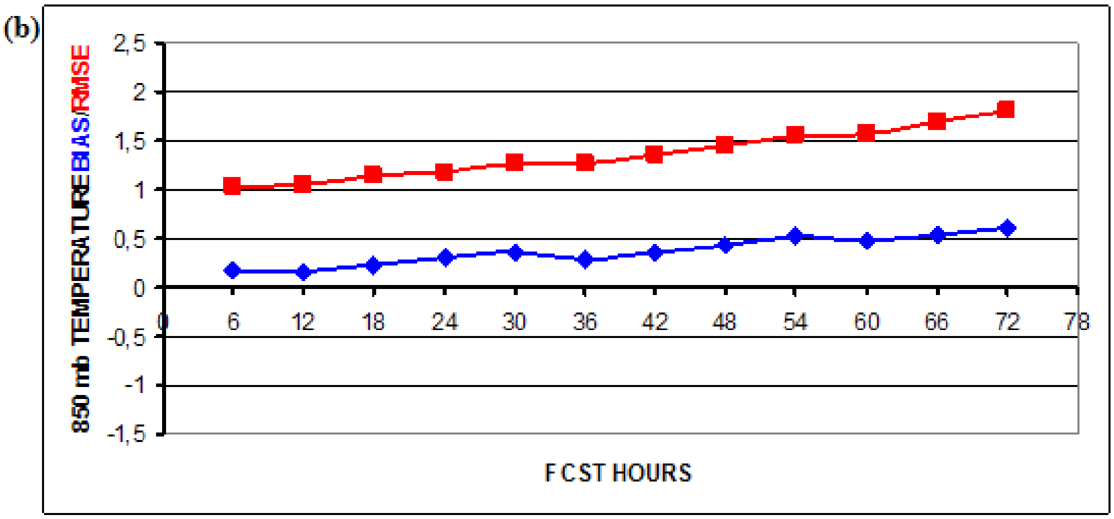

Figure 15. *Bias (blue line) and RMSE (red line) of the 850 mb temperature (℃) forecasts of Aladin/MFSTEP in the Mediterranean sea region in SVP period using a) MF and b) ECMWF gridded analyses.*

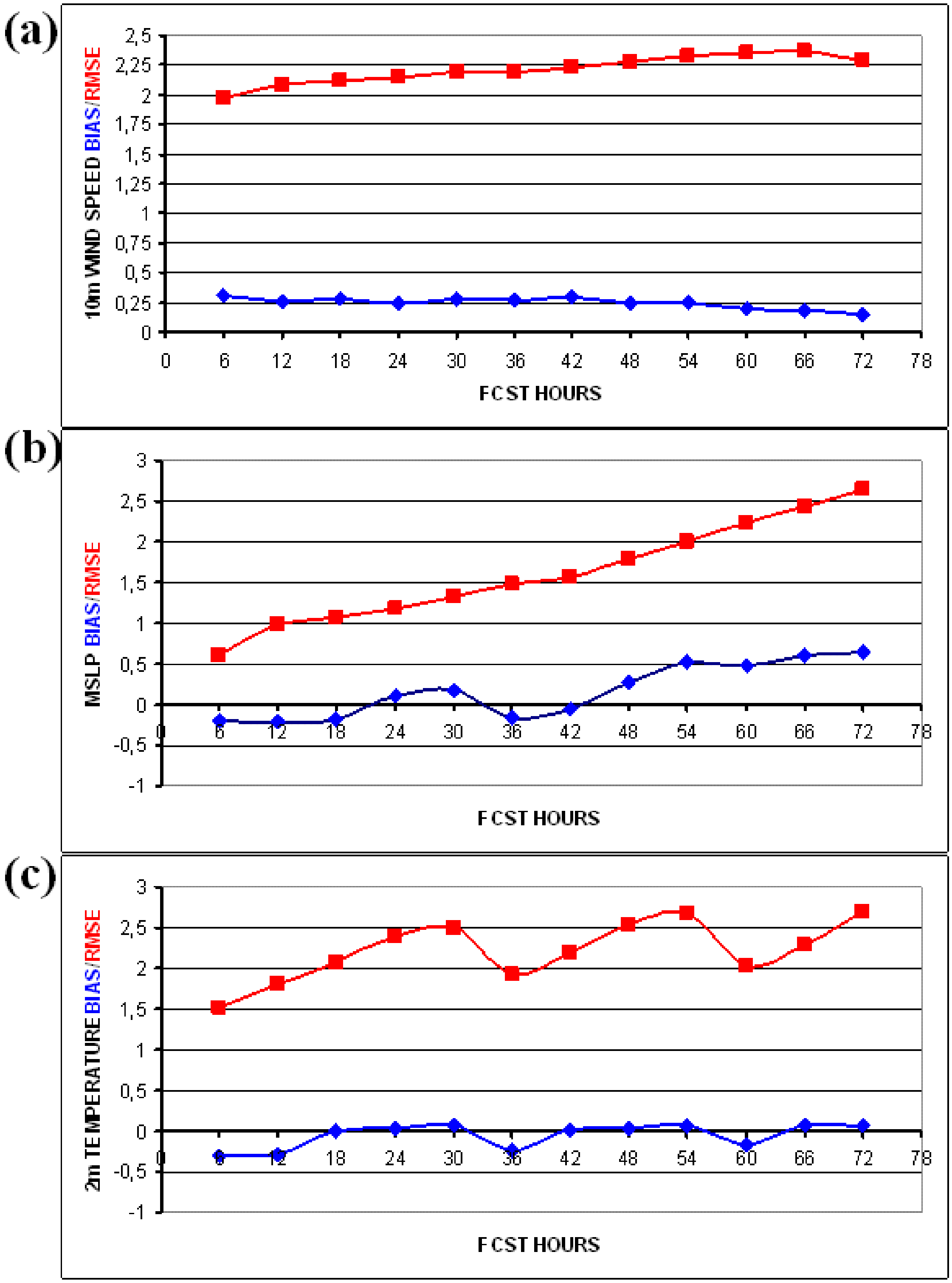

Figure 16. *Bias (blue line) and RMSE (red line) of the Aladin/MFSTEP SVP forecasts in the Mediterranean sea region of a) 10m wind speed (m/s), b) MSLP (hPa) and c) 2m Temperature (℃) using ECMWF gridded analyses.*

(a)
(b)

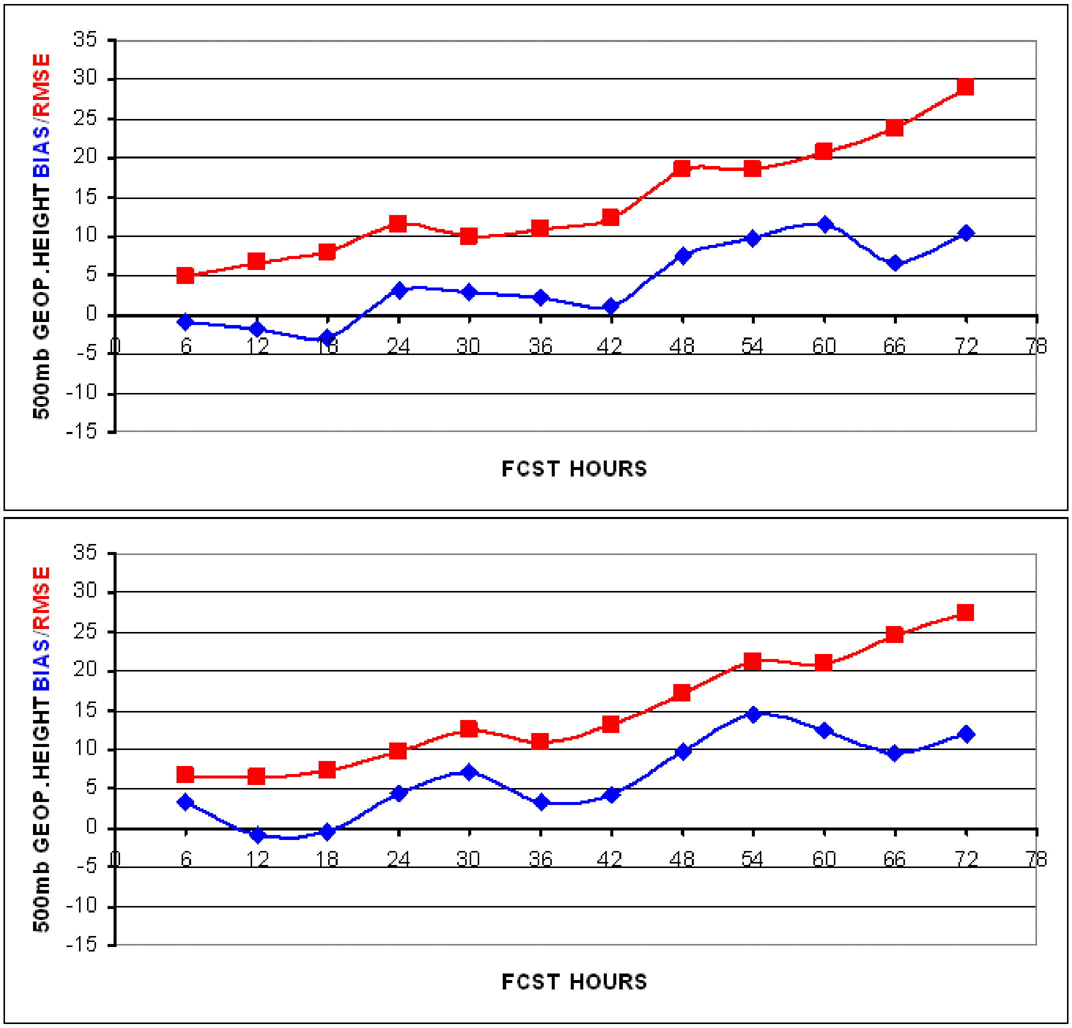

Figure 17. *Bias (blue line) and RMSE (red line) of the 500 mb geopotential height (gpm) forecasts of Aladin/MFSTEP in the Black sea region in SVP period using a) MF and b) ECMWF gridded analyses.*

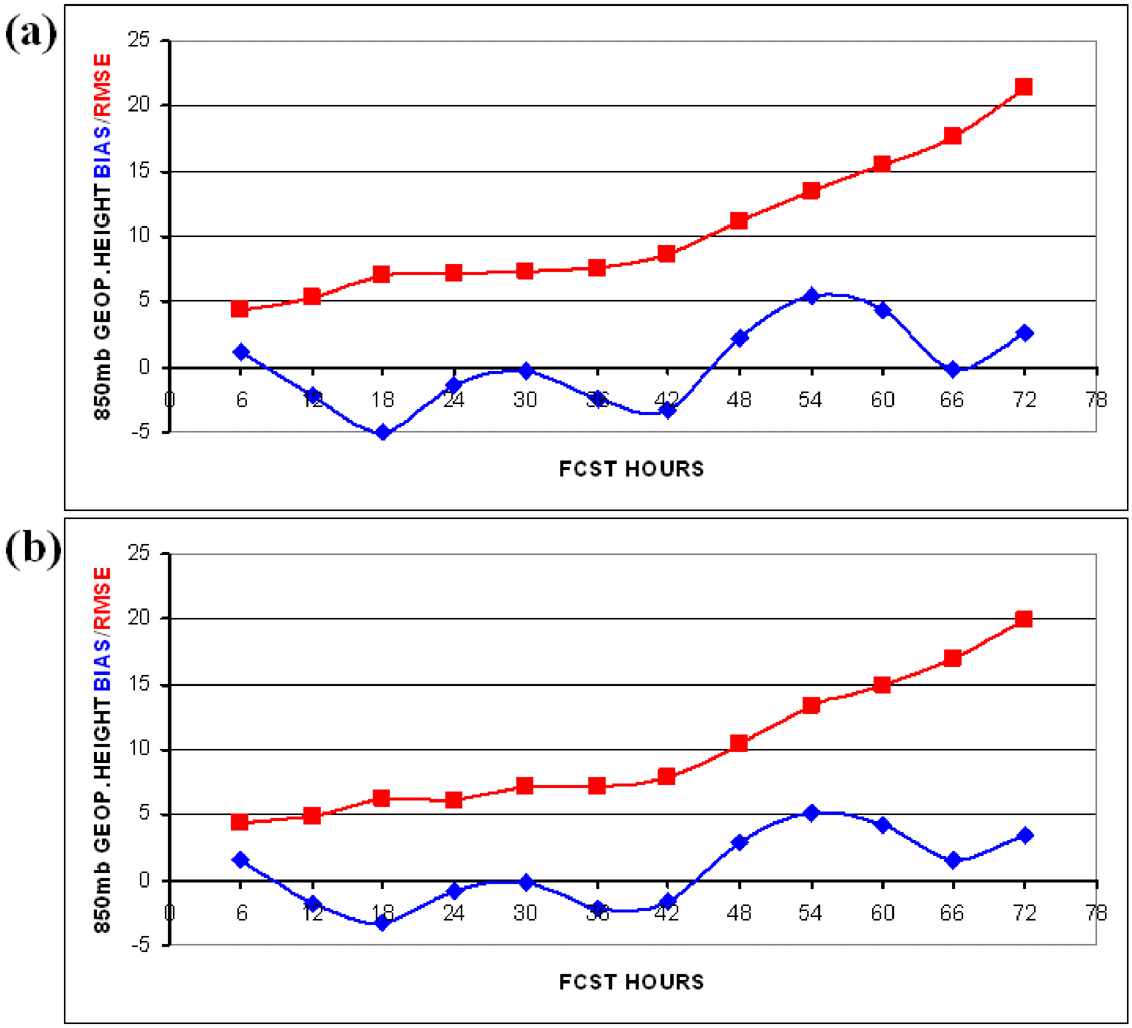

Figure 18. *Bias (blue line) and RMSE (red line) of the 850 mb geopotential height (gpm) forecasts of Aladin/MFSTEP in the Black sea region in SVP period using a) MF and b) ECMWF gridded analyses.*

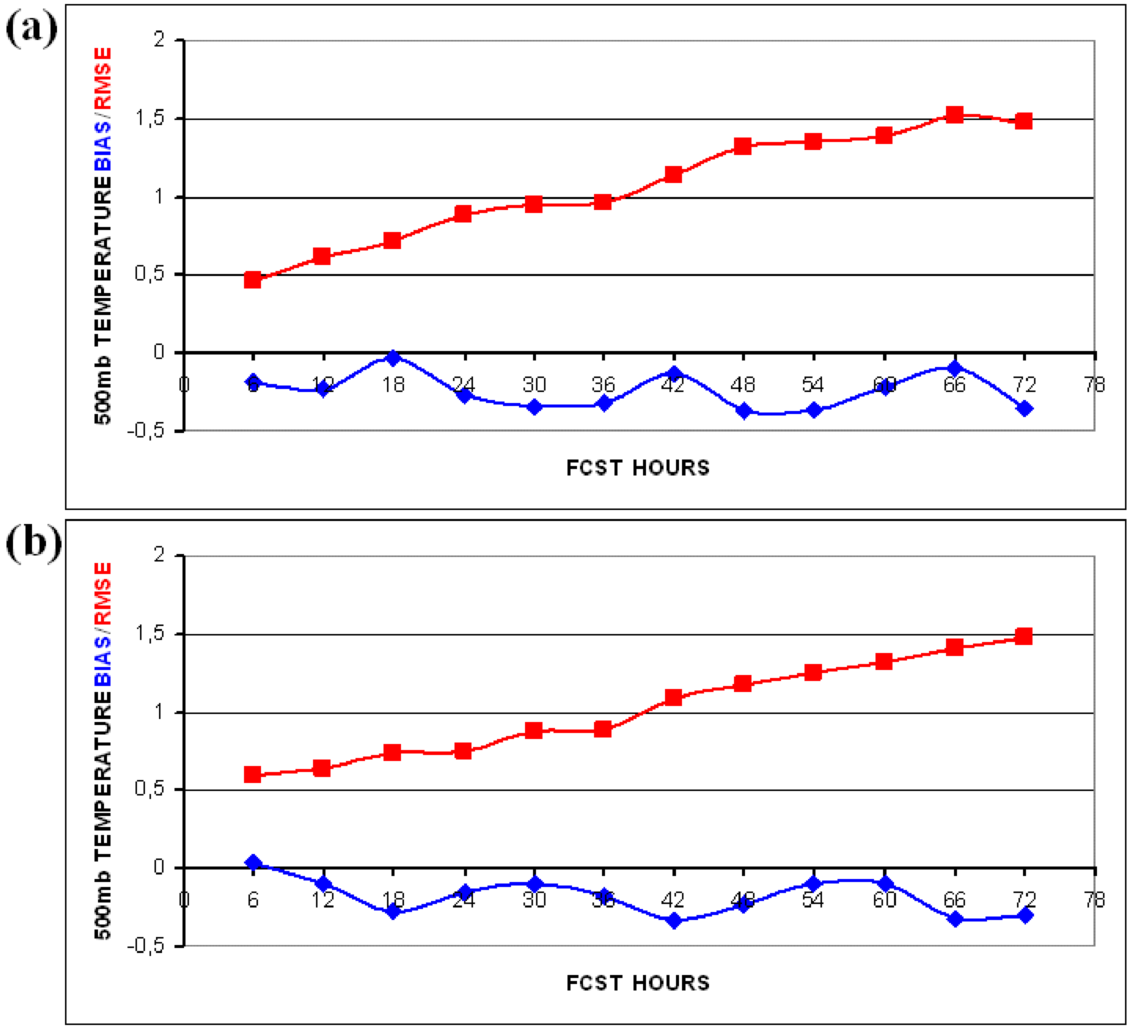

Figure 19. *Bias (blue line) and RMSE (red line) of the 500 mb temperature (℃) forecasts of Aladin/MFSTEP in the Black sea region in SVP period using a) MF and b) ECMWF gridded analyses.*

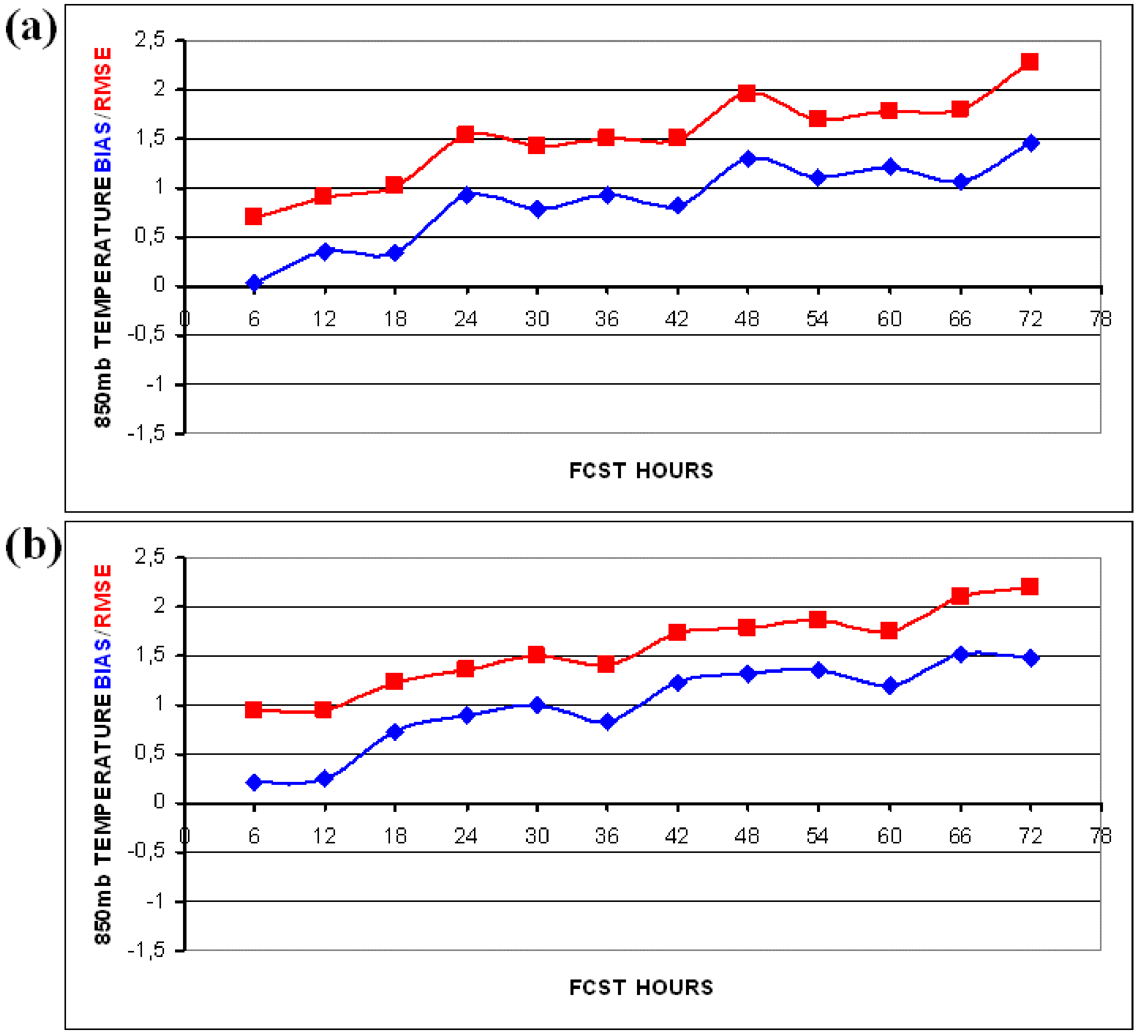

Figure 20. *Bias (blue line) and RMSE (red line) of the 850 mb temperature (℃) forecasts of Aladin/MFSTEP in the Black sea region in SVP period using a) MF and b) ECMWF gridded analyses.*

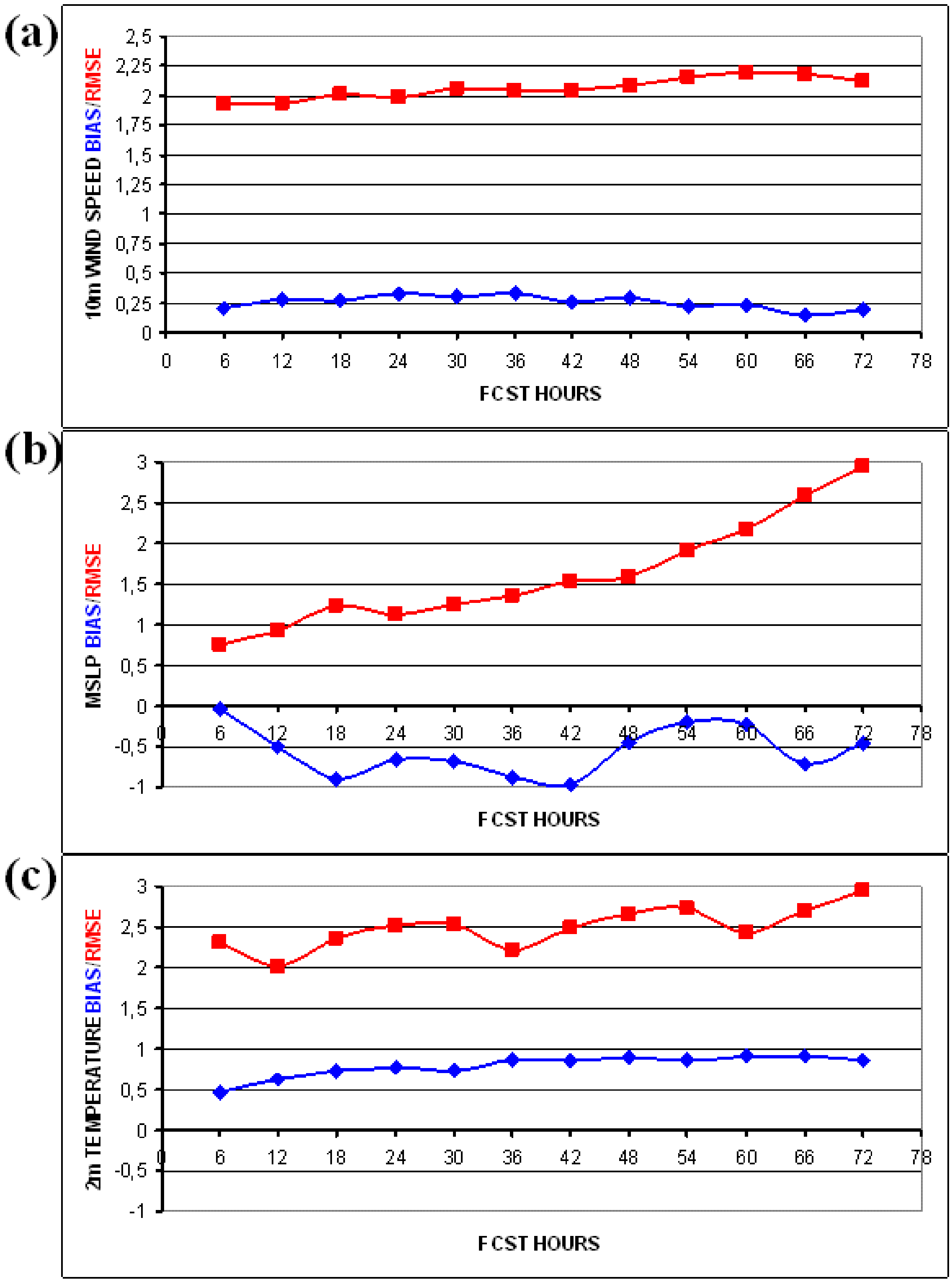

Figure 21. *Bias (blue line) and RMSE (red line) of the Aladin/MFSTEP SVP forecasts in the Black sea region of a) 10m wind speed (m/s), b) MSLP (hPa) and c) 2m Temperature (°C) using ECMWF gridded analyses.*

5.3 NMM

The verification statistics BIAS and RMSE for the NMM model validation against MF analyses for the upper-air parameters are presented in Table 2, and against ECMWF analyses for the surface parameters in Table 3. Model temperature shows quite a good agreement with the MF analyses, on both levels 850 mb and 500 mb, with the average RMSE less then 1.3 º and 0.9 ºK, respectively (Figure 22). Model slightly underestimates geopotential on both 500 mb and 850 mb level, with average RMSE less then 10 m for both levels (Figure 23). Model does not show any systematic bias for the wind components, and has the average RMSE less then 4.5 m/s (Figures 24, 25). Model shows the best scores for the +24 H forecast for all surface parameters (Figure 26). Comparison of the time-series for the surface parameters shows the peak in all scores on 4th January, while in the time series of upper-level data there is a systematic peak on 27th January. Validation scores have been significantly influenced by these two days results.

BIAS	T 500 (K)	T 850 (K)	G 500 (m)	G 850 (m)	U 500 (m/s)	U 850 (m/s)	V 500 (m/s)	V 850 (m/s)	Q 500 (gr/gr)	Q 850(gr/gr)
06 GMT	-0,4	-0,5	-0,4	0,6	-1,8	0,1	0,0	0,7	-0,00001	-0,0002
12 GMT	-0,4	-0,1	-3,9	-2,4	-1,8	-0,5	0,2	0,4	0,00002	-0,0001
18 GMT	-0,4	-0,4	-5,2	-2,1	-1,7	0,2	0,2	0,7	0,000005	-0,0002
24 GMT	-0,3	-0,5	-3,2	-2,1	-1,7	0,2	0,2	0,7	0,000005	-0,0002

RMSE	T 500 (K)	T 850 (K)	G 500 (m)	G 850 (m)	U 500 (m/s)	U 850 (m/s)	V 500 (m/s)	V 850 (m/s)	Q 500 (gr/gr)	Q 850(gr/gr)
06 GMT	0,69	1,06	6,19	5,53	3,82	3,29	3,98	3,66	0,0002	0,001
12 GMT	0,78	1,29	8,75	8,63	4,10	3,11	4,29	3,43	0,0002	0,001
18 GMT	1,00	1,35	11,49	10,26	4,29	3,63	4,68	4,10	0,0002	0,001
24 GMT	0,99	1,44	12,21	11,18	4,63	4,20	4,94	4,48	0,0003	0,001

Table 2. *Verification of the NMM upper-air fields for the SVP period (1-31 Jan 2003) based on comparison with MF analysis.*

BIAS	T 2m (K)	U 10m (m/s)	V 10m (m/s)	MSL (hPa)
06 GMT	-2,5	-0,1	0,5	0,2
12 GMT	3,6	0,5	0,7	-0,9
18 GMT	-0,5	-0,1	0,3	-0,5
24 GMT	-2,5	0,0	0,4	3,5

RMSE	T 2m (K)	U 10m (m/s)	V 10m (m/s)	MSL (hPa)
06 GMT	4,7	2,6	2,6	2,4
12 GMT	6,1	3,6	3,7	4,0
18 GMT	3,7	3,9	4,1	5,1
24 GMT	4,5	2,2	2,2	2,0

Table 3. *Verification of the NMM surface fields for the SVP period (1-31 Jan 2003) based on comparison with ECMWF analysis.*

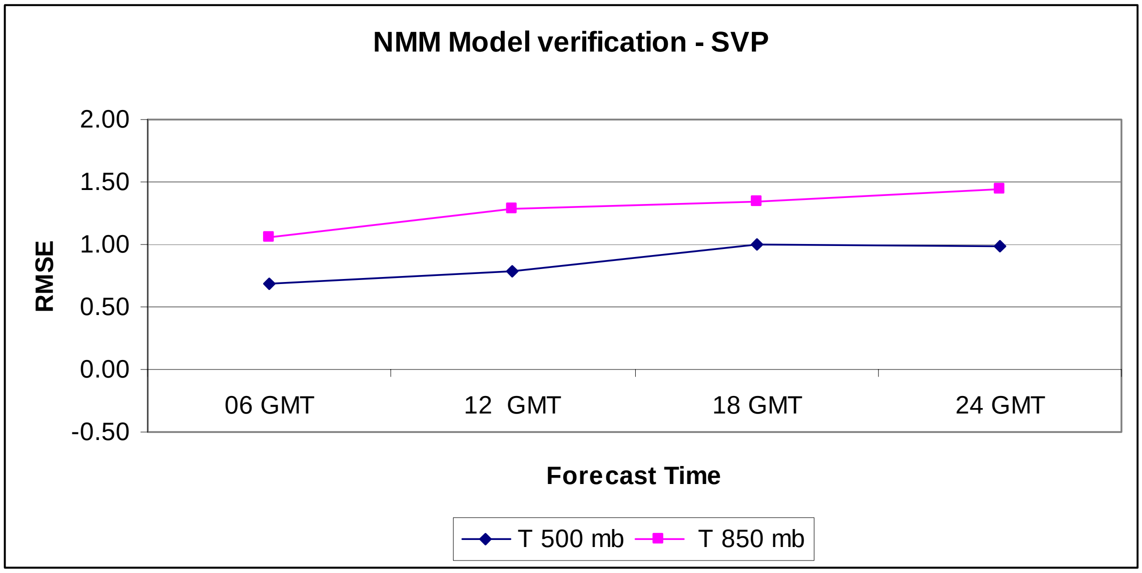

Figure 22. *RMSE of the 500 mb temperature (blue line) and 850 mb temperature (pink line) forecasts of NMM in SVP period using MF gridded analyses.*

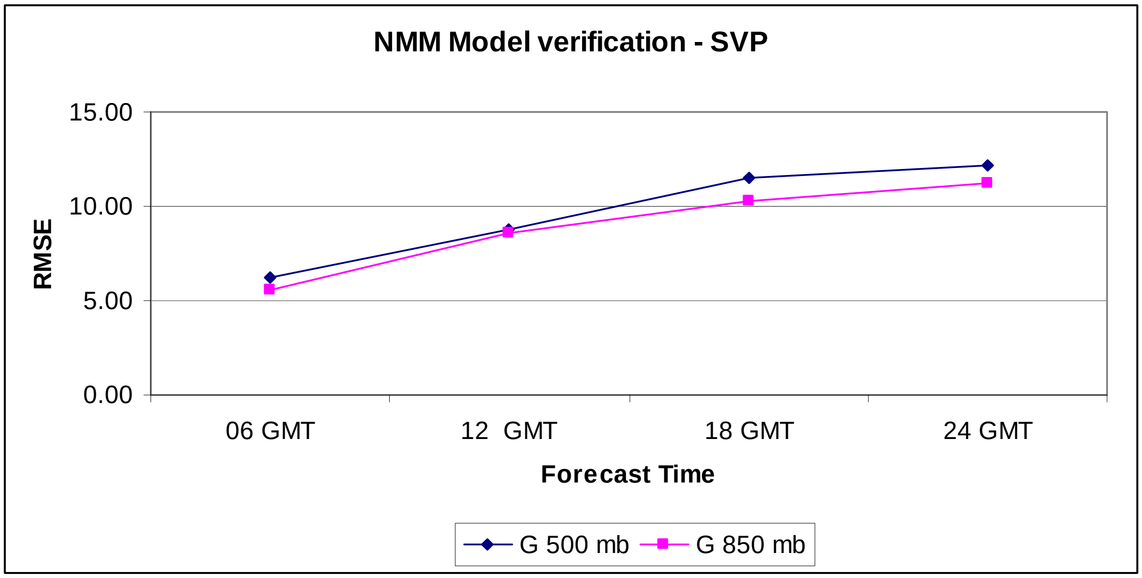

Figure 23. *RMSE of the 500 mb geopotential height (blue line) and 850 mb geopotential height (pink line) forecasts of NMM in SVP period using MF gridded analyses.*

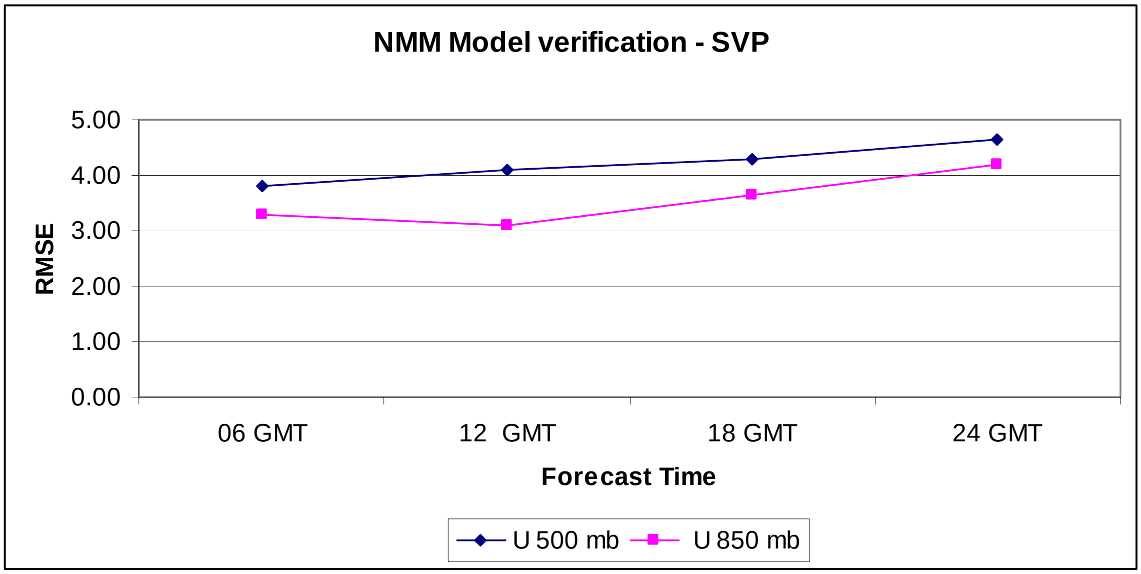

Figure 24. *RMSE of the 500 mb U wind component (blue line) and 850 mb U wind component (pink line) forecasts of NMM in SVP period using MF gridded analyses.*

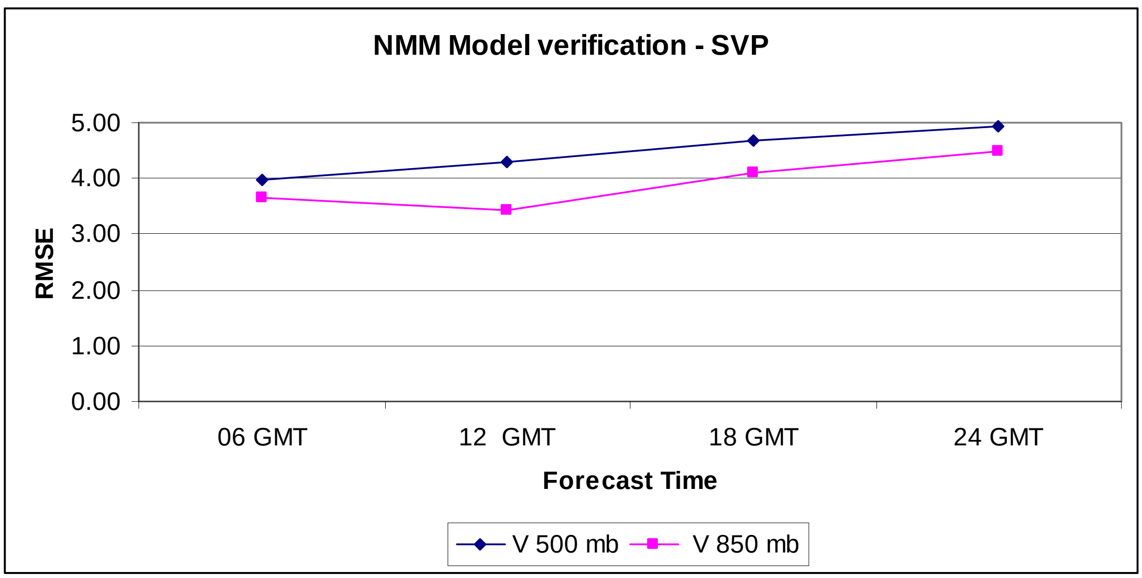

Figure 25. *RMSE of the 500 mb V wind component (blue line) and 850 mb V wind component (pink line) forecasts of NMM in SVP period using MF gridded analyses.*

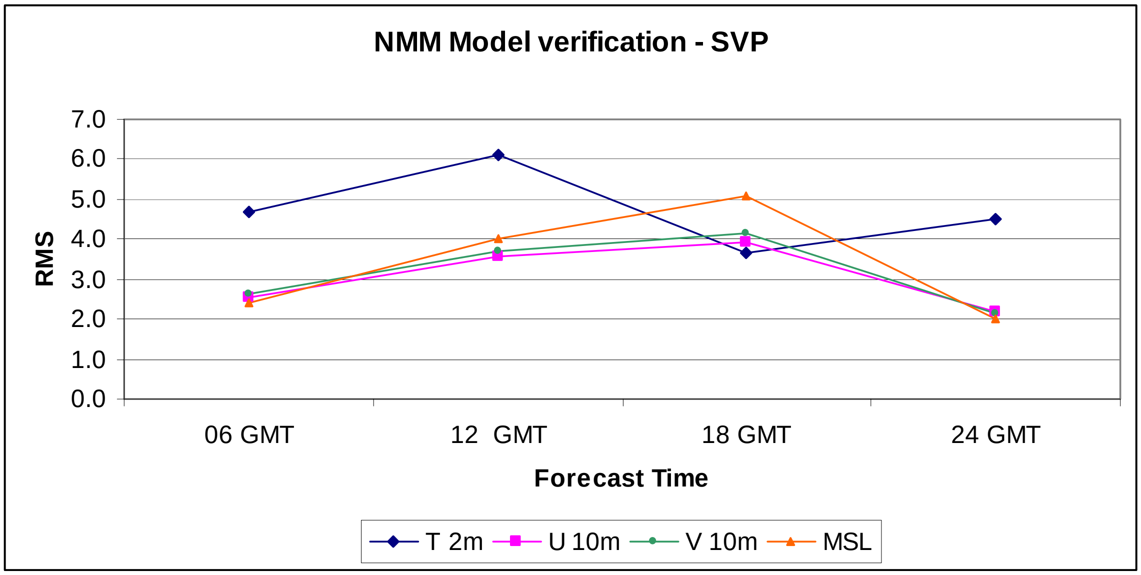

Figure 26. *RMSE of the 2m Temperature (blue line), 10m U wind component (pink line), 10m V wind component (cyan line) and mean sea-level pressure (orange line) forecasts of NMM in SVP period using ECMWF gridded analyses.*

6 Conclusions - Discussion

The evaluation showed that the atmospheric modelling systems used in MFSTEP project were generally consistent on their basic characteristics. Very good forecast skill was exhibited by the two main modelling systems (LAM1-Aladin and LAM2-SKIRON/Eta) in predicting the near-surface properties. Special attention was given to the model predictions near the surface because the surface fields were used by the wave and ocean models of the MFSTEP project. Regarding these parameters in the Mediterranean sea region, the statistical analysis showed that the SKIRON/Eta and Aladin skill scores were close, with the forecasts of SKIRON/Eta being slightly better than those of Aladin. The highest errors appeared in the prediction of the near-surface fields by NMM model. The validation scores of this model were significantly influenced by its low performance in two days (4 and 27 January 2003). Furthermore, negligible differences appeared in the various statistical scores when the SKIRON/Eta and Aladin models were evaluated against different gridded analyses (MF or ECMWF).

Regarding the importance of the non-hydrostatic dynamics in the atmospheric forecasts, Janjic et al. (2001) argued that in the hydrostatic limit the forecasts of traditional meteorological parameters obtained using the hydrostatic and the non-hydrostatic modes are almost indistinguishable. The impact of the non-hydrostatic dynamics appears to be weak at horizontal resolutions larger than about 8 km. This happens because at coarser horizontal resolutions the ratio of the vertical to the horizontal length scale is less than one, the vertical acceleration term can be eliminated from the vertical momentum equation and therefore the hydrostatic assumption becomes valid. Experiments with SKIRON/Eta model for extreme weather events (e.g. meteorological bomb) using different resolutions indicated similar results. The horizontal resolution that was utilized by the atmospheric limited area models in the TOP and SVP runs was about 10 km. Therefore, a further detailed investigation of the impact of the non-hydrostatic dynamics was not necessary. An indirect indication of the weak impact of non-hydrostatic dynamics in the TOP and SVP runs is provided by the fact that the non-hydrostatic SKIRON/Eta and the hydrostatic Aladin/MFSTEP forecasts exhibited very close skill scores.

References

Adcroft, A., C. Hill and J. Marshall, 1997: Representation of topography by shaved cells in a height coordinate ocean model. *Mon. Wea. Rev.*, **125**, 2293–2315.

Ames, W. F., 1969: Numerical Methods for Partial Differential Equations. *Nelson*, London, 291 pp.

Arakawa, A. and V. R. Lamb, 1977: Computational design of the basic dynamical processes of the UCLA general circulation model. *Methods in Computational Physics, 17, Academic Press*, 173-265.

Bénard, P., A. Marki, P.N. Neytchev and M.T. Prtenjak, 2000: Stabilisation of non-linear vertical diffusion schemes in the context of NWP models. Mon. Wea. Rev., 128, 1937-1948.

Berre, L., 2000: Estimation of synoptic and mesoscale forecast error covariances in a limited area model. Mon. Wea. Rev., 128, 644-667.

Boer, G.J., N.A. McFarlane, R. Laprise, J.D. Henderson and J.-P. Blanchet, 1984: The Canadian Climate Centre spectral atmospheric General Circulation Model. Atmosphere-Ocean, 22, 397-429.

Bougeault, P., 1985: A simple parameterization of the large-scale effects of cumulus convection. Mon. Wea. Rev., 113, 2108-2121.

Bouteloup, Y., 1995: Improvement of the spectral representation of the earth topography with a variational method. Mon. Wea. Rev., 123, 1560-1573.

Bubnova, R., G. Hello, P. Bénard and J.-F. Geleyn, 1995: Integration of the fully elastic equations cast in the hydrostatic pressure terrain-following coordinate in the framework of the Aladin NWP system. Mon. Wea. Rev., 123, 515-535.

Côté, J. and A. Staniforth, 1988: A two-time-level semi-Lagrangian semi-implicit scheme for spectral models. Mon. Wea. Rev., 116, 2003-2012.

Davies, H.C., 1976: A lateral boundary formulation for multi-level prediction models. Q.J.R. Meteorol. Soc., 102, 405-418.

Dorman J. L. and P. J. Sellers, 1989: A global climatology of albedo, roughness and stomatal resistance for atmospheric general circulation models as represented by the Simple Biosphere Model (SiB). J. Appl. Meteorol., **28**, 833-855.

Gadd, A. J., 1974: An economical explicit integration scheme. *Meteorological Office* Techn. Note 44, 7 pp. [London Road, Bracknell, Berks. RG12 2SZ, U.K.]

Gallus W. A., Jr., 2000: The Impact of Step Orography on Flow in the Eta Model: Two Contrasting Examples. *Weather and Forecasting*:, **15**, 630–639.

Gallus W. A., Jr. and J. B. Klemp, 2000: Behavior of Flow over Step Orography. *Mon. Wea. Rev.,* **128**, 1153–1164.

Geleyn, J.-F. and A. Hollingworth, 1979: An economical analytical method for the computation of the interaction between scattering and line absorption of radiation. Beitr. Phys. Atmosph., 52, 1-16.

Geleyn, J.-F., C. Girard and J.-F. Louis, 1982: A simple parameterization of moist convection for large-scale atmospheric models. Beitr. Phys. Atmos., 55, 325-334.

Geleyn, J.-F., 1985: On a simple, parameter-free partition between moistening and precipitation in the Kuo scheme. Mon. Wea. Rev., 113, 405-407.

Geleyn, J.-F., 1987: Use of a modified Richardson number for parameterising the effect of shallow convection. J. Met. Soc. Japan, Special 1986 NWP Symposium Issue, 141-149.

Giard, D. and E. Bazile, 2000: Implementation of a new assimilation scheme for soil and surface variables in a global NWP model. Mon. Wea. Rev., **128**, 997-1015.

Hortal, M., 2002: The development and testing of a new two-time-level semi-Lagrangian scheme (SETTLS) in the ECMWF forecast model. Q. J. R. Meteorol. Soc., 128, 1671-1688.

Janjic, Z.I., 1974: A stable centered difference scheme free of the two-grid-interval noise. *Monthly Weather Review*, **102**, 319-323.

_________, 1977: Pressure gradient force and advection scheme used for forecasting with steep and small scale topography. *Contributions to Atmospheric Physics*, **50**, 186–199.

_________, 1979: Forward–backward scheme modified to prevent two–grid–interval noise and its application in sigma coordinate models. *Contributions to Atmospheric Physics*, **52**, 69–84.

_________, 1984: Non–linear advection schemes and energy cascade on semi–staggered grids. *Mon. Wea. Rev.*, **112**, 1234–1245.

_________, 1990: The step–mountain coordinate: physical package. *Mon.Wea.Rev.*, **118**, 1429–1443.

_________, 1994: The step–mountain eta coordinate model: further developments of the convection, viscous sublayer and turbulence closure schemes. *Mon. Wea. Rev.*, **122**, 927–945.

_________, 1996: The Surface Layer Parameterization in the Eta Model. Third Summer School in Meteorology, Krivaja, Yugoslavia. Lecture notes, pp. 53.

Janjic, Z. and A. Wiin–Nielsen, 1977: On geostrophic adjustment and numerical procedures in a rotating fluid. *J. Atmos. Sci.*, **34**, 297–310.

Janjic, Z. I., J. P. Gerrity, Jr. and S. Nickovic, 2001: An Alternative Approach to Nonhydrostatic Modeling. *Monthly Weather Review*, Vol. **129**

Janjic, Z. I., and G. DiMego, 2001: Effects of Mountain Representation and Nonhydrostatic Dynamics in a Case of Orographic Precipitation. Preprints, Symposium on Precipitation Extremes: Prediction, Impacts and Responses. 81st Annual Meeting of the American Meteorological Society, January 14-19, 2001, Albuquerque, NM, AMS, Boston, MA

Kallos, G., 1997: The Regional weather forecasting system SKIRON. Proceedings of the Symposium on Regional Weather Prediction on Parallel Computer Environments, 15-17 October 1997, Athens, Greece. pp 9.

Kallos, G., S. Nickovic, D. Jovic, O. Kakaliagou, A. Papadopoulos, N. Misirlis, L. Boukas, N. Mimikou, 1997: The ETA model operational forecasting system and its parallel implementation. Proceedings of the 1st Workshop on Large-Scale Scientific Computations, 7-11 June, Varna, Bulgaria, pp 15.

Kallos, G., A. Voudouri, I. Pytharoulis, and O. Kakaliagou, 2001: Modeling the mercury cycle in the Mediterranean: similarities and differences with conventional air pollution modeling. 25th ITM NATO/CCMS on Air Pollution Modeling and its Application, Louvain-la-Neuve, Belgium, 67-74.

Katsafados, P., 2003: Factors and parameterizations that determine the performance of limited area models in long-range weather forecasts. PhD Thesis, Dept. of Physics, Univ. of Athens, Athens, Greece. pp. 257 (in Greek).

Kessler, E., 1969: On the distribution and continuity of water substance in atmospheric circulation. Atmos. Meteor. Monograph, Vol. 32, 84 pp.Laprise, R., 1992: The Euler equations of motion with hydrostatic pressure as an independent variable. Mon. Wea. Rev., 120, 197-207.

Lindzen, R.S., 1981: Turbulence and stress owing to gravity wave and tidal breakdown. J. Geophys. Res., 86, 9707-9714.

Liu, W.T., K.B. Katsaros and J.A. Businger, 1979: Bulk parametrization of air-sea exchanges of heat and water vapor including the molecular constraints at the interface. *J. Atmos. Sci.,* **36**, 1722-1735.

Lott, F. and M. Miller, 1997: A new subgrid scale orographic drag parameterization; its testing in the ECMWF model. Q. J. R. Meteorol. Soc., 123, 101-127.

Lott, F., 1999: Alleviation of stationary biases in a GCM through a mountain drag parameterization scheme and a simple representation of lift forces. Mon. Wea. Rev., 127, 788-801.

Louis, J.-F., 1979: A parametric model of vertical eddy fluxes in the atmosphere. Boundary-layer Meteorol., 17, 187-202.

Louis, J.-F., M. Tiedke and J.-F. Geleyn, 1981: A short history of the operational PBL-parameterization at ECMWF. ECMWF Workshop Proceedings on «Planetary boundary layer parameterizations», 25-27 November 1981, 59-79.

Lynch, P., D. Giard and V. Ivanovici, 1997: Improving the efficiency of a digital filtering scheme. Mon. Wea. Rev., 125, 1976-1982.

McDonald, A., 1998: The origin of noise in semi-Lagrangian integrations. ECMWF Seminar Procedings on «Recent developments in numerical methods for atmospheric modelling», 7-11 September 1998, 308-334.

Machenhauer, B. and J.E. Haugen, 1987: Test of a spectral limited area shallow water model with time dependent lateral boundary conditions and combined normal mode/semi-Lagrangian time integration schemes. ECMWF Workshop Proceedings on «Techniques for horizontal discretisation in numerical prediction models», 2-4 November 1987, 361-377.

Mangarella, P.A., A.J. Chambers, R.L. Street, and E.Y. Hsu, 1973: Laboratory studies of evaporation and energy transfer through a wavy air-water interface. *J. Phys. Oceanogr*., **3**, 93-101.

Mellor, G.L. and T. Yamada, 1982: Development of a turbulence closure model for geophysical fluid problems. *Rev. Geophys. Space Phys.,* **20**, 851-875.

Mesinger, F., 1984: A blocking technique for representation of mountains in atmospheric models. Riv. Meteor. Aeronaut., **44**, 195-202.

Mesinger, F., Z.I. Janjic, S. Nickovic, D. Gavrilov and D.G. Deaven, 1988: The step–mountain coordinate: model description and performance for cases of Alpine lee cyclogenesis and for a case of an Appalachian redevelopment. *Mon.Wea. Rev.*, **116**, 1493–1518.

Nickovic, S., D. Mihailovic, B. Rajkovic and A. Papadopoulos, 1998: The Weather Forecasting System SKIRON, Vol. II: Description of the Model, Department of Physics, University of Athens, pp. 228

Nickovic, S., G. Kallos, A. Papadopoulos and O. Kakaliagou, 2001: A model for prediction of desert dust cycle in the atmosphere. J. Geoph. Res., **106,** 18113-18129.

Noilhan, J. and S. Planton, 1989: A simple parameterization of land surface processes for meteorological models. Mon. Wea. Rev., 117, 536-549.

Papadopoulos, A., P. Katsafados, and G. Kallos, 2002: Regional weather forecasting for marine application. GAOS, **8**, No 2-3, 219-237.

Radnoti, G., 1995: Comments on «A spectral limited-area formulation with time-dependent boundary conditions applied to the shallow-water equations». Mon. Wea. Rev., 123, 3122-3123.

Ritchie, H., C. Temperton, A. Simmons, M. Hortal, T. Davies, D. Dent and M. Hamrud, 1995: Implementation of the semi-Lagrangian method in a high-resolution version of the ECMWF forecast model. Mon. Wea. Rev., 123, 489-514.

Ritchie, H. and M. Tanguay, 1996: A comparison of spatially-averaged Eulerian and semi-Lagrangian treatments of mountains. Mon. Wea. Rev., 124, 167-181.

Ritter, B. and J.-F. Geleyn, 1992: A comprehensive radiation scheme for numerical weather prediction models with potential applications in climate simulations. Mon. Wea. Rev., 120, 303-325.

Simmons, A. and D. Burridge, 1981: An energy and angular momentum conserving vertical finite-difference scheme and hybrid vertical coordinates. Mon. Wea. Rev., 109, 2003-2012.

Simmons, A. and C. Temperton, 1997: Stability of a two-time-level semi-implicit integration scheme for gravity wave motions. Mon. Wea. Rev., 125, 600-615.

Staudenmeier, M., Jr. and J. Mittelstadt, 1998: Results of the Western Region evaluation of the Eta-10 Model. Preprints, Twelfth Conference on Numerical Weather Prediction, Phoenix, AZ, 11-16 January, 1998; AMS, Boston, MA, 131-134.

Temperton, C., 1997: Treatment of the Coriolis terms in semi-Lagrangian spectral models. Special 'André Robert Memorial Volume' Issue of Atmosphere-Ocean, Numerical methods in atmospheric and oceanic modelling, 293-302.

Thiebaux, J., E. Rogers, W. Wang, and B. Katz, 2003: A new high-resolution blended real-time global sea surface temperature analysis. Bull. Amer. Meteor. Soc., **84**, 645-656.

Voudouri, A., I. Pytharoulis and G. Kallos, 2005: Mercury budget estimates for the State of New York. EFM, **5**, 87-107.

Wilks, D.S., 1995: Statistical Methods in the Atmospheric Sciences, Academic Press NY, pp. 467.

Winninghoff, F. J., 1968: On the adjustment toward a geostrophic balance in a simple primitive equation model with application to the problems of initialization and objective analysis. Ph. D. Thesis, *Dept. Meteor. Univ. California*. "Dept. Meteor. Univ. California, Los Angeles, CA 90024, U.S.A.'

Zhao, Q., and F.H. Carr, 1997: A prognostic cloud scheme for operational NWP models. *Mon. Wea. Rev.,* **125**, 1931-1953.

Zilitinkevich, S.S., 1995: Non-local turbulent transport: pollution dispersion aspects of coherent structure of convective flows. In*: Air Pollution III - Volume I. Air Pollution Theory and Simulation* (Eds. H. Power, N. Moussiopoulos and C.A. Brebbia). Computational Mechanics Publications, Southampton Boston, 53-60.

Zobler, L., 1986: A world soil file for global climate modeling. *NASA Thechn. Memo. 87802.*